

# MAKING NETWORKS ROBUST TO COMPONENT FAILURE

A Dissertation Outline Presented

by

DANIEL P. GYLLSTROM

Submitted to the Graduate School of the  
University of Massachusetts Amherst in partial fulfillment  
of the requirements for the degree of

DOCTOR OF PHILOSOPHY

(Compiled on 02/07/2013 at 11:51)

Computer Science

© Copyright by Daniel P. Gyllstrom 2012

All Rights Reserved

# MAKING NETWORKS ROBUST TO COMPONENT FAILURE

A Dissertation Outline Presented

by

DANIEL P. GYLLSTROM

Approved as to style and content by:

---

Jim Kurose, Chair

---

Prashant Shenoy, Member

---

Deepak Ganesan, Member

---

Lixin Gao, Member

---

Lori Clarke, Department Chair  
Computer Science

# ABSTRACT

## MAKING NETWORKS ROBUST TO COMPONENT FAILURE

(COMPILED ON 02/07/2013 AT 11:51)

DANIEL P. GYLLSTROM

B.Sc., TRINITY COLLEGE

M.Sc., UNIVERSITY OF MASSACHUSETTS AMHERST

Ph.D., UNIVERSITY OF MASSACHUSETTS AMHERST

Directed by: Professor Jim Kurose

Communication network components – routers, links connecting routers, and sensors – inevitably fail, causing service outages and a potentially unusable network. Recovering quickly from these failures is vital to both reducing short-term disruption and increasing long-term network survivability. In this thesis, we consider instances of component failure in the Internet and in networked cyber-physical systems, such as the communication network used by the modern electric power grid (termed the *smart grid*). We design algorithms that make these networks more robust to component failure. This thesis divides into three parts: (a) recovery from malicious or misconfigured nodes injecting false information into a distributed system (e.g., the Internet), (b) placing smart grid sensors to provide measurement error detection, and (c) fast recovery from link failures in a smart grid communication network.

First, we consider the problem of malicious or misconfigured nodes that inject and spread incorrect state throughout a distributed system. Such false state can degrade the performance of a distributed system or render it unusable. For example, in the case of network routing algorithms, false state corresponding to a node incorrectly declaring a cost of 0 to all destinations (maliciously or due to misconfiguration) can quickly spread through the network. This causes other nodes to (incorrectly) route via the misconfigured node, resulting in suboptimal routing and network congestion. We propose three algorithms for efficient recovery in such scenarios and evaluate their efficacy.

The last two parts of this thesis consider robustness in the context of the electric power grid. We study a type of sensor, a Phasor Measurement Unit (PMU), currently being deployed in electric power grids worldwide. PMUs provide voltage and current measurements at a sampling rate orders of magnitude higher than the status quo. As a result, PMUs can both drastically improve existing power grid operations and enable an entirely new set of applications, such as the reliable integration of renewable energy resources. However, PMU applications require *correct* (addressed in thesis part 2) and *timely* (covered in thesis part 3) PMU data. Without these guarantees, smart grid operators and applications may make incorrect decisions and take corresponding (incorrect) actions.

The second part of this thesis addresses PMU measurement errors, which have been observed in practice. We formulate a set of PMU placement problems that aim to satisfy two constraints: place PMUs “near” each other to allow for measurement error detection and use the minimal number of PMUs to infer the state of the maximum number of system buses and transmission lines. For each PMU placement problem, we prove it is NP-Complete, propose a simple greedy approximation algorithm, and evaluate our greedy solutions.

Lastly, we design algorithms for fast recovery from link failures in a smart grid communication network. This is a two-part problem: (a) link detection failure and (b) algorithms for pre-computing backup multicast trees. To address (a), we design link-detection failure and reporting mechanisms that use OpenFlow to detect link failures when and where they occur *inside* the network. OpenFlow is an open source framework that cleanly separates the control and data planes for use in network management and control. For part (b), we propose a set of algorithms that precompute backup multicast trees to be used after a link failure. Each algorithm aims to minimize end-to-end packet loss and delay but each uses different optimization criteria to achieve this goal: minimize control overhead, minimize the number of affected flows across all multicast trees, and minimize the number of affected sink nodes across all multicast trees. We implement and evaluate these algorithms in Openflow.

# TABLE OF CONTENTS

	Page
<b>ABSTRACT</b> .....	<b>iv</b>
<b>LIST OF TABLES</b> .....	<b>x</b>
<b>LIST OF FIGURES</b> .....	<b>xi</b>
 <b>CHAPTER</b>	
<b>INTRODUCTION</b> .....	<b>1</b>
0.1 Thesis Overview .....	1
0.1.1 Component Failure in Communication Networks .....	1
0.1.2 Approaches to Making Networks More Robust to Failures .....	2
0.2 Thesis Contributions .....	4
0.3 Thesis Outline .....	6
 <b>1. RECOVERY FROM FALSE ROUTING STATE IN     DISTRIBUTED ROUTING ALGORITHMS</b> .....	 <b>7</b>
1.1 Introduction .....	7
1.2 Problem Formulation .....	9
1.3 Recovery Algorithms .....	10
1.3.1 Preprocessing Algorithm .....	11
1.3.2 The 2 <sup>nd</sup> best Algorithm .....	11
1.3.3 The purge Algorithm .....	11
1.3.4 The cpr Algorithm .....	12
1.4 Analysis of Algorithms .....	12
1.5 Simulation Study .....	13
1.5.1 Simulations using Graphs with Fixed Link Weight .....	15
1.5.2 Simulations using Graphs with Changing Link Weights .....	16

1.5.3	Summary of Simulation Results	18
1.6	Related Work	19
1.7	Conclusions	20
<b>2.</b>	<b>PMU SENSOR PLACEMENT FOR MEASUREMENT ERROR DETECTION IN THE SMART GRID</b>	<b>22</b>
2.1	Introduction	22
2.2	Preliminaries	25
2.2.1	Assumptions, Notation, and Terminology	25
2.2.2	Observability Rules	25
2.2.3	Cross-Validation Rules	26
2.3	Four NP-Complete PMU Placement Problems	26
2.3.1	Overview of NPC Proof Strategy	27
2.3.2	Problem Statements and NPC Proof Sketches	29
2.4	Approximation Algorithms	31
2.5	Simulation Study	32
2.6	Related Work	34
2.7	Conclusions	36
<b>3.</b>	<b>RECOVERY FROM LINK FAILURES IN A SMART GRID COMMUNICATION NETWORK</b>	<b>37</b>
3.1	Introduction	37
3.2	Background and Related Work	39
3.2.1	PMU Applications and Their QoS Requirements	39
3.2.2	OpenFlow	40
3.2.3	Related Work	41
3.2.3.1	Smart Grid Communication	41
3.2.3.2	Detecting Packet Loss	42
3.2.3.3	Multicast Tree Recovery	43
3.3	Proposed Research	45
3.3.1	Preliminaries	46
3.3.1.1	Example Scenario	46
3.3.1.2	General Problem Scenario and Basic Notation	46
3.3.2	Overview of Our Recovery Solutions and Section Outline	49



3.3.3	Link Failure Detection using OpenFlow .....	51
3.3.4	Uninstalling Failed Trees and Installing Backup Trees .....	54
3.3.5	Computing Backup Multicast Trees .....	55
3.3.5.1	MIN-FLOWS Algorithm .....	55
3.3.5.2	MIN-SINKS Algorithm .....	57
3.3.5.3	MIN-CONTROL Algorithm .....	58
3.4	Chapter Conclusion and Future Work .....	59
<b>4.</b>	<b>THESIS TIMELINE AND FUTURE WORK .....</b>	<b>61</b>
4.1	Planned Future Work and Timeline .....	61
4.2	Future Work Outside the Scope of this Thesis .....	62
	<b>BIBLIOGRAPHY .....</b>	<b>64</b>

## LIST OF TABLES

Table	Page
1.1 Average number pairwise routing loops for 2ND-BEST in simulation described in Section 1.5.1. ....	15
3.1 PMU applications and their QoS requirements. The $\heartsuit$ refers to reference [17] and $\triangle$ to [7]. ....	40

## LIST OF FIGURES

Figure		Page
1.1	Message overhead as function of the number of hops false routing state has spread from the compromised node ( $k$ ), over Erdős-Rényi graphs with fixed link weights. The Erdős-Rényi graphs are generated using $n = 100$ , and $p = .05$ , yielding an average diameter of 6.14. ....	16
1.2	Section 1.5.2 plots. Both plots consider Erdős-Rényi graphs with changing link costs generated using $n = 100$ and $p = .05$ . The average diameter of the generated graphs is 6.14. ....	18
2.1	The figure in (a) shows $G(\varphi) = (V(\varphi), E(\varphi))$ using example formula, $\varphi$ , from Equation (2.1). (b) shows the new graph formed by replacing each variable node in $G(\varphi)$ – as specified by the Theorem 2.1 proof – with the Figure 2.2(a) variable gadget. ....	29
2.2	Gadgets used in Theorem 2.1 - 2.4. $Z_i$ in Figure 2.2(a), $Z_i^t$ in Figure 2.2(c), and $Z_i^b$ in Figure 2.2(c) are the only zero-injection nodes. The dashed edges in Figure 2.2(a) and Figure 2.2(c) are connections to clause gadgets. Likewise, the dashed edges in Figure (b) are connections to variable gadgets. In Figure 2.2(c), superscript, $t$ , denotes nodes in the upper subgraph and superscript, $b$ , indexes nodes in the lower subgraph. ....	30
2.3	Mean number of observed nodes over synthetic graphs based on IEEE bus 57 when varying number of PMUs. The 90% confidence interval is shown. ....	35
3.1	Example used in Section 3.3.2. The shaded nodes are members of the source-based multicast tree rooted at $a$ . The lightly shaded nodes are not a part of the multicast tree. ....	47

# INTRODUCTION

Communication network components (routers, links, and sensors) fail. These failures can cause widespread network service disruption and outages, and potentially critical errors for network applications. *In this thesis, we examine how networks – traditional networks and networked cyber-physical systems, such as the smart grid – can be made more robust to component failure.*

We propose on-demand recovery algorithms for distributed network algorithms that optimize for control message overhead and convergence time, and preplanned approaches to recovery for electric power grid applications, where reliability is key. An electric power grid consists of a set of buses - electric substations, power generation centers, or aggregation points of electrical loads - and transmission lines connecting those buses. We refer to modern and future electric power grids that automate power grid operations using sensors and wide-area communication as the *smart grid*.

## 0.1 Thesis Overview

### 0.1.1 Component Failure in Communication Networks

In this thesis, we consider three separate but related problems: node (i.e., switch or router) failure in traditional networks such as the Internet or wireless sensor networks, the failure of critical sensors that measure voltage and current throughout the smart grid, and link failures in a smart grid communication network. For distributed network algorithms, a malicious or misconfigured node can inject and spread incorrect state throughout the distributed system. Such false state can degrade the performance of the network or render it unusable. For example, in 1997 a significant portion of Internet traffic was routed through a single misconfigured router that had

spread false routing state to several Internet routers. As a result, a large portion of the Internet became inoperable for several hours [40].

In particular, component failure in a smart grid can be catastrophic. For example, if smart grid sensors or links in its supporting communication network fail, smart grid applications can make incorrect decisions and take corresponding (incorrect) actions. Critical smart grid applications required to operate and manage a power grid are especially vulnerable to such failures because typically these applications have strict data delivery requirements, needing both ultra low latency and assurance that data is received correctly. In the worst case, component failure can lead to a cascade of power grid failures like the August 2003 blackout in the USA [2] and the recent power grid failures in India [50].

### **0.1.2 Approaches to Making Networks More Robust to Failures**

For many distributed systems, recovery algorithms operate on-demand (as opposed to being preplanned) because algorithm and system state is typically distributed throughout the network of nodes. As a result, fast convergence time and low control message overhead are key requirements for efficient recovery from component failure. In order to make the problem of on-demand recovery in a distributed system concrete, we investigate distance vector routing as an instance of this problem where nodes must recover from incorrectly injected state information. Distance vector forms the basis for many routing algorithms widely used in the Internet (e.g., BGP, a path-vector algorithm) and in multi-hop wireless networks (e.g., AODV, diffusion routing).

In the first technical chapter of this thesis, we design, develop, and evaluate three different approaches for correctly recovering from the injection of false distance vector routing state (e.g., a compromised node incorrectly claiming a distance of 0 to all destinations). Such false state, in turn, may propagate to other routers through the normal execution of distance vector routing, causing other nodes to (incorrectly) route

via the misconfigured node, making this a network-wide problem. Recovery is correct if the routing tables in all nodes have converged to a global state in which all nodes have removed each compromised node as a destination, and no node has a least cost path to any destination that routes through a compromised node.

The second and third thesis chapters consider robustness from component failure specifically in the context of the smart grid. Because reliability is a key requirement for the smart grid, we focus on preplanned approaches to failure recovery.

In our second thesis chapter, we study a type of sensor, a Phasor Measurement Unit (PMU), currently being deployed in electric power grids worldwide. PMUs provide voltage and current measurements at a sampling rate orders of magnitude higher than the status quo. As a result, PMUs can both drastically improve existing power grid operations and enable an entirely new set of applications, such as the reliable integration of renewable energy resources. We formulate a set of problems that consider PMU measurement errors, which have been observed in practice. Specifically, we specify four PMU placement problems that aim to satisfy two constraints: place PMUs “near” each other to allow for measurement error detection and use the minimal number of PMUs to infer the state of the maximum number of system buses and transmission lines. For each PMU placement problem, we prove it is NP-Complete, propose a simple greedy approximation algorithm, and evaluate our greedy solutions.

In our final technical thesis chapter, we present the initial design for algorithms that provide recovery from link failures in a smart grid communication network. The recovery problem divides into two parts: (a) link failure detection and (b) algorithms for pre-computing backup multicast trees. To address (a), we sketch the design of a link-failure detection and reporting mechanisms that use OpenFlow to detect link failures when and where they occur *inside* the network. OpenFlow is an open source framework that cleanly separates the control and data planes for use in centralized network management and control. For part (b), we propose initial outlines for a set of

algorithms that precompute backup multicast trees to be installed after a link failure. As future work, we plan to implement these algorithms in Openflow and evaluate them.

## 0.2 Thesis Contributions

The main contributions of this thesis are:

- We design, develop, and evaluate three different algorithms – 2ND-BEST, PURGE, and CPR – for correctly recovering from the injection of false routing state in distance vector routing. 2ND-BEST performs localized state invalidation, followed by network-wide recovery using the traditional distance vector algorithm. PURGE first globally invalidates false state and then uses distance vector routing to recompute distance vectors. CPR takes and stores local routing table snapshots at each router, and then uses a rollback mechanism to implement recovery. We prove the correctness of each algorithm for scenarios of single and multiple compromised nodes.
- We use simulations and analysis to evaluate 2ND-BEST, PURGE, and CPR in terms of control message overhead and convergence time. We find that 2ND-BEST performs poorly due to routing loops. Over topologies with fixed link costs, PURGE performs nearly as well as CPR even though our simulations and analysis assume near perfect conditions for CPR. Over more realistic scenarios in which link weights can change, we find that PURGE yields lower message complexity and faster convergence time than CPR and 2ND-BEST.
- We define four PMU placement problems, three of which are completely new, that place PMUs at a subset of electric power grid buses. Two PMU placement problems consider measurement error detection by requiring PMUs to be placed “near” each other to allow for their measurements to be cross-validated. For

each PMU placement problem, we prove it is NP-Complete and propose a simple greedy approximation algorithm.

- We prove our greedy approximations for PMU placement are correct and give complexity bounds for each. Through simulations over synthetic topologies generated using real portions of the North American electric power grid as templates, we find that our greedy approximations yield results that are close to optimal: on average, within 97% of optimal. We also find that imposing our requirement of cross-validation to ensure PMU measurement error detection comes at small marginal cost: on average, only 5% fewer power grid buses are observed (covered) when PMU placements require cross-validation versus placements that do not.
- We propose initial approaches for algorithms that perform preplanned recovery from link failures in a smart grid communication network. Our proposed research divides into two parts: link failure detection and algorithms for pre-computing backup multicast trees. For the first part, we design algorithms that use OpenFlow to detect and report link failures when and where they occur, *inside* the network. To address the second part, we propose a set of algorithms that compute backup multicast trees that are installed after a link failure. Each algorithm computes a backup multicast tree that aims to minimize end-to-end packet loss and delay, but each algorithm uses different optimization criteria in achieving this goal: minimizing control overhead, minimizing the number of affected flows across all multicast trees, and minimizing the number of affected sink nodes across all multicast trees. These optimization criteria differ from those proposed in the literature.



### **0.3 Thesis Outline**

The rest of this thesis proposal is organized as follows. We present algorithms for recovery from false routing state in distributed routing algorithms in Chapter 1. In Chapter 2 we formulate PMU placement problems that provide measurement error detection. Chapter 3 presents our initial and proposed research on efficient recovery from link failures in a smart grid communication network. We conclude by outlining planned future work in Chapter 4.

# CHAPTER 1

## RECOVERY FROM FALSE ROUTING STATE IN DISTRIBUTED ROUTING ALGORITHMS

### 1.1 Introduction

Malicious and misconfigured nodes can degrade the performance of a distributed system by injecting incorrect state information. Such false state can then be further propagated through the system either directly in its original form or indirectly, e.g., by diffusing computations initially using this false state. In this chapter, we consider the problem of removing such false state from a distributed system.

In order to make the false-state-removal problem concrete, we investigate distance vector routing as an instance of this problem. Distance vector forms the basis for many routing algorithms widely used in the Internet (e.g., BGP, a path-vector algorithm) and in multi-hop wireless networks (e.g., AODV, diffusion routing). However, distance vector is vulnerable to compromised nodes that can potentially flood a network with false routing information, resulting in erroneous least cost paths, packet loss, and congestion. Such scenarios have occurred in practice. For example, in 1997 a significant portion of Internet traffic was routed through a single misconfigured router, rendering a large part of the Internet inoperable for several hours [40]. Distance vector currently has no mechanism to recover from such scenarios. Instead, human operators are left to manually reconfigure routers. It is in this context that we propose and evaluate automated solutions for recovery.

In this chapter, we design, develop, and evaluate three different approaches for correctly recovering from the injection of false routing state (e.g., a compromised node

incorrectly claiming a distance of 0 to all destinations). Such false state, in turn, may propagate to other routers through the normal execution of distance vector routing, making this a network-wide problem. Recovery is correct if the routing tables in all nodes have converged to a global state in which all nodes have removed each compromised node as a destination, and no node has a least cost path to any destination that routes through a compromised node.

Specifically, we develop three novel distributed recovery algorithms: 2ND-BEST, PURGE, and CPR. 2ND-BEST performs localized state invalidation, followed by network-wide recovery. Nodes directly adjacent to a compromised node locally select alternate paths that avoid the compromised node; the traditional distributed distance vector algorithm is then executed to remove remaining false state using these new distance vectors. The PURGE algorithm performs global false state invalidation by using diffusing computations to invalidate distance vector entries (network-wide) that routed through a compromised node. As in 2ND-BEST, traditional distance vector routing is then used to recompute distance vectors. CPR uses snapshots of each routing table (taken and stored locally at each router) and a rollback mechanism to implement recovery. Although our solutions are tailored to distance vector routing, we believe they represent approaches that are applicable to other diffusing distributed computations.

For each algorithm, we prove correctness, derive communication complexity bounds, and evaluate its efficiency in terms of message overhead and convergence time via simulation. Our analysis and simulations show that when considering topologies in which link costs remain fixed, CPR outperforms both PURGE and 2ND-BEST (at the cost of checkpoint memory). This is because CPR can efficiently remove all false state by simply rolling back to a checkpoint immediately preceding the injection of false routing state. In scenarios where link costs can change, PURGE outperforms CPR and 2ND-BEST. CPR performs poorly because, following rollback, it must process

the valid link cost changes that occurred since the false routing state was injected; 2ND-BEST and PURGE, however, can make use of computations subsequent to the injection of false routing state that did not depend on the false routing state. We will see, however, that 2ND-BEST performance suffers because of the so-called count-to-infinity problem.

Recovery from false routing state has similarities to the problem of recovering from malicious transactions [6, 35] in distributed databases. Our problem is also similar to that of rollback in optimistic parallel simulation [32]. However, we are unaware of any existing solutions to the problem of recovering from false routing state. A related problem to the one considered in this chapter is that of discovering misconfigured nodes. In Section 1.2, we discuss existing solutions to this problem. In fact, the output of these algorithms serve as input to the recovery algorithms proposed in this chapter.

This chapter has six sections. In Section 1.2 we define the false-state-removal problem and state our assumptions. We present our three recovery algorithms in Section 1.3. Then, in Section 1.4, we briefly state the results of our message complexity analysis. Section 1.5 describes our simulation study. We detail related work in Section 1.6 and conclude the chapter in Section 1.7. The research described here has been published in [28].

## 1.2 Problem Formulation

We consider distance vector routing [10] over arbitrary network topologies. We model a network as an undirected graph,  $G = (V, E)$ , with a link weight function  $w : E \rightarrow \mathbb{N}$ . Each node,  $v$ , maintains the following state as part of distance vector: a vector of all adjacent nodes ( $adj(v)$ ), a vector of least cost distances to all nodes in  $G$  ( $\overrightarrow{min_v}$ ), and a *distance matrix* that contains distances to every node in the network via each adjacent node ( $dmatrix_v$ ).

We assume that the identity of the compromised node is provided by a different algorithm, and thus do not consider this problem in this paper. Examples of such algorithms include [21, 22, 24] in the context of wired networks and [44] in the wireless setting. Specifically, we assume that at time  $t$ , this algorithm is used to notify all neighbors of the compromised node(s). Let  $t'$  be the time the node was compromised.

For each of our algorithms, the goal is for all nodes to recover “correctly”: all nodes should remove the compromised node as a destination and find new least cost distances that do not use the compromised node. If the network becomes disconnected as a result of removing the compromised node, all nodes need only compute new least cost distances to all other nodes within their connected component.

For simplicity, let  $\bar{v}$  denote the compromised node, let  $\overrightarrow{old}$  refer to  $\overrightarrow{min_{\bar{v}}}$  before  $\bar{v}$  was compromised, and let  $\overrightarrow{bad}$  denote  $\overrightarrow{min_{\bar{v}}}$  after  $\bar{v}$  has been compromised.

### 1.3 Recovery Algorithms

In this section we propose three recovery algorithms: 2ND-BEST, PURGE, and CPR. With one exception, the input and output of each algorithm is the same:<sup>1</sup>

- Input: Undirected graph,  $G = (V, E)$ , with weight function  $w : E \rightarrow \mathbb{N}$ .  $\forall v \in V$ ,  $\overrightarrow{min}$  and  $dmatrix$  are computed (using distance vector). Also, each  $v \in adj(\bar{v})$  is notified that  $\bar{v}$  was compromised.
- Output: Undirected graph,  $G' = (V', E')$ , where  $V' = V - \{\bar{v}\}$ ,  $E' = E - \{(\bar{v}, v_i) \mid v_i \in adj(\bar{v})\}$ , and link weight function  $w : E \rightarrow \mathbb{N}$ .  $\overrightarrow{min_v}$  and  $dmatrix_v$  are computed via the algorithms discussed below  $\forall v \in V'$ .

Before we describe each recovery algorithm, we outline a preprocessing procedure common to all three recovery algorithms.

---

<sup>1</sup>Additionally, as input CPR requires that each  $v \in adj(\bar{v})$  is notified of the time,  $t'$ , in which  $\bar{v}$  was compromised.

### 1.3.1 Preprocessing Algorithm

All three recovery algorithms share a common preprocessing procedure. The procedure removes  $\bar{v}$  as a destination and finds the node IDs in each connected component. This could be implemented (as we have done here) using diffusing computations [20] initiated at each  $v \in adj(\bar{v})$ . In our case, each diffusing computation message contains a vector of node IDs. When a node receives a diffusing computation message, the node adds its ID to the vector and removes  $\bar{v}$  as a destination. At the end of the diffusing computation, each  $v \in adj(\bar{v})$  has a vector that includes all nodes in  $v$ 's connected component. Finally, each  $v \in adj(\bar{v})$  broadcasts the vector of node IDs to all nodes in their connected component. In the case where removing  $\bar{v}$  partitions the network, each node will only compute shortest paths to nodes in the vector.

### 1.3.2 The 2<sup>nd</sup> best Algorithm

2ND-BEST invalidates state locally and then uses distance vector to implement network-wide recovery. Following the preprocessing described in Section 1.3.1, each neighbor of the compromised node locally invalidates state by selecting the least cost pre-existing alternate path that does not use the compromised node as the first hop. The resulting distance vectors trigger the execution of traditional distance vector to remove the remaining false state.

2ND-BEST is simple and makes no synchronization assumptions. However, 2ND-BEST is vulnerable to the count-to-infinity problem. Because each node only has local information, the newly selected shortest paths may continue to use  $\bar{v}$ . We will see in our simulation study that the count-to-infinity problem can incur significant message and time costs.

### 1.3.3 The purge Algorithm

PURGE globally invalidates all false state using a diffusing computation and then uses distance vector to compute new distance values that avoid all invalidated paths.

The diffusing computation is initiated at the neighbors of  $\bar{v}$  because only these nodes are aware if  $\bar{v}$  is used as an intermediary node. The diffusing computations spread from  $\bar{v}$ 's neighbors to the network edge, invalidating false state at each node along the way. Then ACKs travel back from the network edge to the neighbors of  $\bar{v}$ , indicating that the diffusing computation is complete. Next, PURGE uses distance vector to recompute least cost paths invalidated by the diffusing computations.

#### 1.3.4 The cpr Algorithm

CPR<sup>2</sup> is our third and final recovery algorithm. Unlike 2ND-BEST and PURGE, CPR requires that clocks across different nodes be loosely synchronized i.e., the maximum clock offset between any two nodes is bounded. Here we present CPR assuming all clocks are perfectly synchronized.

For each node,  $i \in G$ , CPR adds a time dimension to  $\overrightarrow{min}_i$  and  $dmatrix_i$ , which CPR then uses to locally archive a complete history of values. Once the compromised node is discovered, the archive allows each node to rollback to a system snapshot from a time before  $\bar{v}$  was compromised. CPR does so using diffusing computations. Then, CPR removes all  $\overrightarrow{bad}$  and  $\overrightarrow{old}$  state while updating stale distance values resulting from link cost changes that occurred between the time the snapshot was taken and the “current” time. This last step is executed by initiating a distance vector computation from the neighbors of the compromised node.

### 1.4 Analysis of Algorithms

Here we summarize the results from our analysis. The detailed proofs can be found in our corresponding technical report [29]. Using a synchronous communication model, we derive communication complexity bounds for each algorithm. Our analysis assumes: a graph with unit link weights of 1, that only a single node is compromised,

---

<sup>2</sup>The name is an abbreviation for **C**heck**P**oint and **R**ollback.

and that the compromised node falsely claims a cost of 1 to every node in the graph. For graphs with fixed link costs, we find that the communication complexity of all three algorithms is bounded above by  $O(mnd)$  where  $d$  is the diameter,  $n$  is the number of nodes, and  $m$  the maximum out-degree of any node.

In the second part of our analysis, we consider graphs where link costs can change. Again, we assume a graph with unit link weights of 1 and a single compromised node that declares a cost of 1 to every node. Additionally, we let link costs increase between the time the malicious node is compromised and the time at which error recovery is initiated. We assume that across all network links, the total increase in link weights is  $w$  units. We find that CPR incurs additional overhead (not experienced by 2ND-BEST and PURGE) because CPR must update stale state after rolling back. 2ND-BEST and PURGE avoid the issue of stale state because neither algorithm rolls back in time. As a result, the message complexity for 2ND-BEST and PURGE is still bounded by  $O(mnd)$  when link costs can change, while CPR is not. CPR's upper bound becomes  $O(mnd) + O(w n^2)$ .

## 1.5 Simulation Study

In this section, we use simulations to characterize the performance of each of our three recovery algorithms in terms of message and time overhead. Our goal is to illustrate the relative performance of our recovery algorithms over different topologies (e.g., Erdős-Rényi graphs, Internet-like graphs) and across different network conditions (e.g., topologies with fixed link costs, topologies with changing link costs, a single compromised node, and multiple compromised nodes).

We build a custom simulator with a synchronous communication model: nodes send and receive messages at fixed epochs. In each epoch, a node receives a message from all its neighbors and performs its local computation. In the next epoch, the node sends a message (if needed). All algorithms are deterministic under this com-



munication model. The synchronous communication model, although simple, yields interesting insights into the performance of each of the recovery algorithms.

We simulate the following scenario:

1. Before  $t'$ ,  $\forall v \in V$   $\overrightarrow{min}_v$  and  $dmatrix_v$  are correctly computed.
2. At time  $t'$ ,  $\bar{v}$  is compromised and advertises a  $\overrightarrow{bad}$  (a vector with a cost of 1 to *every* node in the network) to its neighboring nodes.
3. The effect of  $\overrightarrow{bad}$  spreads for a specified number of hops (this varies by experiment). The variable  $k$  refers to the number of hops that the effect of  $\overrightarrow{bad}$  has spread.
4. At time  $t$ , some node  $v \in V$  notifies all  $v \in adj(\bar{v})$  that  $\bar{v}$  was compromised.<sup>3</sup>

The message and time overhead are measured in step (4) above. The pre-computation, described in Section 1.3.1, is not counted towards message and time overhead because all three recovery algorithms use this same procedure.

In order to keep this thesis proposal document brief, we only discuss a subset of our simulation results. We focus on a simplified scenario in which a single compromised node has distributed false routing state. We consider Erdős-Rényi graphs in cases where link costs remain fixed (Section 1.5.1) and link costs change (Section 1.5.2). The corresponding technical report [29], discusses results using a richer simulation model that considers more realistic network conditions: an asynchronous communication model, Internet-like graphs generated using GT-ITM [1] and Rocketfuel [3], and multiple compromised nodes. We find that the trends discussed in this report hold when using these new topologies and additional simulation scenarios.

---

<sup>3</sup> For CPR this node also indicates the time,  $t'$ ,  $\bar{v}$  was compromised.

$k = 1$	$k = 2$	$k = 3$	$k = 4 - 10$
554	1303	9239	12641

**Table 1.1.** Average number pairwise routing loops for 2ND-BEST in simulation described in Section 1.5.1.

### 1.5.1 Simulations using Graphs with Fixed Link Weight

Here we evaluate our recovery algorithms, in terms of message and time overhead, using Erdős-Rényi graphs with fixed link weights. In particular, we consider Erdős-Rényi graphs with parameters  $n$  and  $p$ , where  $n$  is the number of graph nodes and  $p$  is the probability that link  $(i, j)$  exists where  $i, j \in V$ . Link weights are selected uniformly at random between  $[1, n]$ .

In order to establish statistical significance, we generate several Erdős-Rényi graphs to be used in our simulations. We iterate over different values of  $k$ . For each  $k$ , we generate an Erdős-Rényi graph,  $G = (V, E)$ , with parameters  $n$  and  $p$ . Then we select a  $v \in V$  uniformly at random and simulate the scenario described above, using  $v$  as the compromised node. In total we sample 20 unique nodes for each  $G$ . We set  $n = 100$ ,  $p = \{0.05, 0.15, 0.25, 0.25\}$ , and let  $k = \{1, 2, \dots, 10\}$ . Each data point is an average over 600 runs (20 runs over 30 topologies).

Figure 1.1 shows the message overhead as a function of  $k$  when  $p = .05$ . The 90% confidence interval is included in the plot. CPR outperforms the other algorithms because CPR removes false routing state with a single diffusing computation, rather than using an iterative process as in 2ND-BEST and PURGE. 2ND-BEST performs poorly because of the count-to-infinity problem: Table 1.1 shows the large average number of pairwise routing loops, an indicator of the occurrence of count-to-infinity problem, 2ND-BEST encounters this simulation. In addition, we counted the number of epochs in which at least one pairwise routing loop existed. For 2ND-BEST (across all topologies), on average, all but the last three timesteps had at least one routing

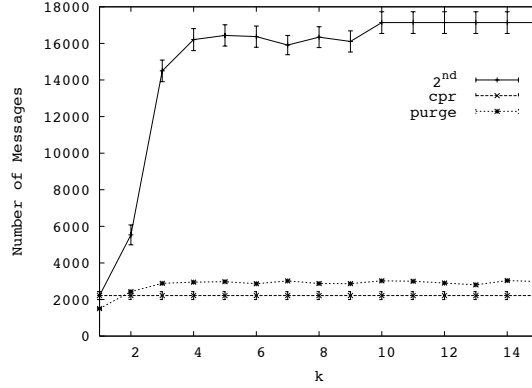


**Figure 1.1.** Message overhead as function of the number of hops false routing state has spread from the compromised node ( $k$ ), over Erdős-Rényi graphs with fixed link weights. The Erdős-Rényi graphs are generated using  $n = 100$ , and  $p = .05$ , yielding an average diameter of 6.14.

loop. This suggests that the count-to-infinity problem dominates the cost for 2ND-BEST. In contrast, no routing loops are found with PURGE or CPR, as expected.

However, CPR’s encouraging results should be interpreted with caution. CPR requires both loosely synchronized clocks and the time that node  $\bar{v}$  was compromised to be identified, assumptions not required by 2ND-BEST nor PURGE. Furthermore, this first simulation scenario is ideal for CPR because fixed link costs ensure minimal stale state (i.e., residual  $\overrightarrow{old}$  state) after CPR rolls back. The next two simulations present more challenging and less favorable conditions for CPR.

### 1.5.2 Simulations using Graphs with Changing Link Weights

In the next two simulations we evaluate our algorithms over graphs with changing link costs. We introduce link cost changes between the time  $\bar{v}$  is compromised and when  $\bar{v}$  is discovered (e.g. during  $[t', t]$ ). In particular, there are  $\lambda$  link cost changes per timestep, where  $\lambda$  is deterministic. To create a link cost change event, we modify links uniformly at random (except for all  $(v, \bar{v})$  links), where the new link cost is selected uniformly at random from  $[1, n]$ .

**Effects of Link Cost Changes.** Except for  $\lambda$ , our simulation setup is identical to that of the previous section. We let  $\lambda = \{1, 4, 8\}$ . In order to isolate the effects of link costs changes, we assume that CPR checkpoints at each timestep.

For the sake of brevity, we only show results for  $n = 100, p = .05, \lambda = 4$  in Figure 1.2(a).<sup>4</sup> PURGE yields the lowest message overhead, but only slightly lower than CPR. CPR’s message overhead increases with larger  $k$  because there are more link cost change events to process. After CPR rolls back, it must process all link cost changes that occurred in  $[t', t]$ . In contrast, 2ND-BEST and PURGE process some of the link cost change events during the interval  $[t', t]$  as part of normal distance vector execution.

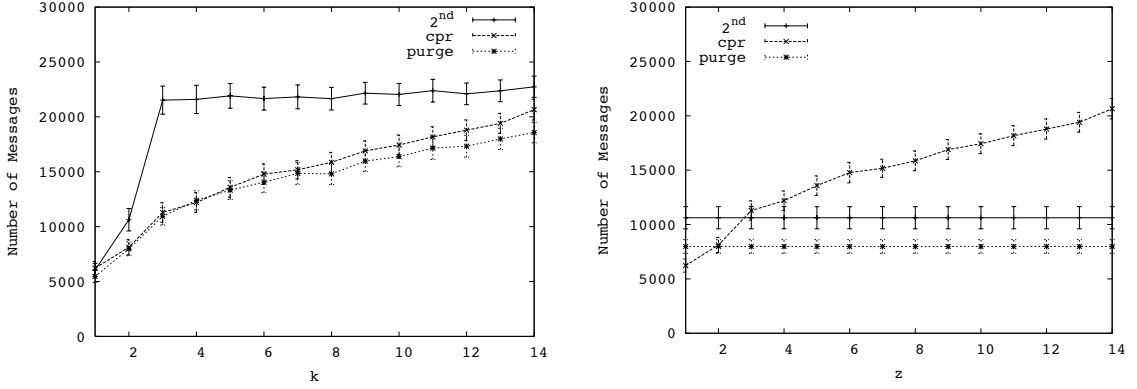
Our analysis further indicates that 2ND-BEST performance suffers because of the count-to-infinity problem. The gap between 2ND-BEST and the other algorithms shrinks as  $\lambda$  increases because link cost changes have a larger effect on message overhead as  $\lambda$  grows.

**Effects of Varying Checkpoint Frequency.** In this simulation, we study the trade-off between message overhead and storage overhead for CPR. To this end, we vary the frequency at which CPR checkpoints and fix the interval  $[t', t]$ . Otherwise, our simulation setup is the same as the one just described (under the title “Effects of Link Cost Changes”).

For conciseness, we only display a single plot. Figure 1.2(b) shows the results for an Erdős-Rényi graph with link weights selected uniformly at random between  $[1, n]$ ,  $n = 100, p = .05, \lambda = 4$  and  $k = 2$ . We plot message overhead against the number of timesteps CPR must rollback,  $z$ . CPR’s message overhead increases with larger  $z$  because as  $z$  increases there are more link cost change events to process. 2ND-BEST and PURGE have constant message overhead because they operate independent of  $z$ .

---

<sup>4</sup>Our simulations for different  $p$  values, yield the same trends. Refer to our technical report for more details [29].



(a) Message overhead as a function of the number of hops false routing state has spread ( $k$ ) where  $\lambda = 4$  link cost changes occur at each timestep. (b) Message overhead as function of varying the checkpoint frequency,  $z$ .  $z = 0$  implies checkpointing occurs at every timestep,  $z = 1$  creates checkpoints every other timestamp, etc.

**Figure 1.2.** Section 1.5.2 plots. Both plots consider Erdős-Rényi graphs with changing link costs generated using  $n = 100$  and  $p = .05$ . The average diameter of the generated graphs is 6.14.

We conclude that as the frequency of CPR snapshots decreases, CPR incurs higher message overhead. Therefore, when choosing the frequency of checkpoints, the trade-off between storage and message overhead must be carefully considered.

### 1.5.3 Summary of Simulation Results

Our results show that for graphs with fixed link costs, CPR yields the lowest message and time overhead. CPR benefits from removing false state with a single diffusing computation. However, CPR has storage overhead, requires loosely synchronized clocks, and requires the time that node  $\bar{v}$  was compromised to be identified.

2ND-BEST's performance is determined by the count-to-infinity problem. PURGE avoids the count-to-infinity problem by first globally invalidating false state. Therefore in cases where the count-to-infinity problem is significant, PURGE outperforms 2ND-BEST.

When considering graphs with changing link costs, CPR's performance suffers because it must process all valid link cost changes that occurred since  $\bar{v}$  was compro-

mised. Meanwhile, 2ND-BEST and PURGE make use of computations that followed the injection of false state, that do not depend on false routing state. However, 2ND-BEST’s performance degrades because of the count-to-infinity problem. PURGE eliminates the count-to-infinity problem and therefore yields the best performance over topologies with changing link costs.

Finally, we found that an additional challenge with CPR is setting the parameter that determines the checkpoint frequency. More frequent checkpointing yields lower message and time overhead at the cost of more storage overhead. Ultimately, application-specific factors must be considered when setting this parameter.

## 1.6 Related Work

To the best of our knowledge no existing approach exists to address recovery from false routing state in distance vector routing. However, our problem is similar to that of recovering from malicious but committed database transactions. Liu et al. [6] and Ammann et al [35] develop algorithms to restore a database to a valid state after a malicious transaction has been identified. PURGE’s algorithm to globally invalidate false state can be interpreted as a distributed implementation of the dependency graph approach by Liu et al. [35]. Additionally, if we treat link cost change events that occur after the compromised node has been discovered as database transactions, we face a similar design decision as in [6]: do we wait until recovery is complete before applying link cost changes or do we allow the link cost changes to execute concurrently?

Database crash recovery [39] and message passing systems [21] both use snapshots to restore the system in the event of a failure. In both problem domains, the snapshot algorithms are careful to ensure snapshots are globally consistent. In our setting, consistent global snapshots are not required for CPR, since distance vector routing only requires that all initial distance estimates be non-negative.

Garcia-Lunes-Aceves’s DUAL algorithm [26] uses diffusing computations to coordinate least cost updates in order to prevent routing loops. In our case, CPR and the preprocessing procedure (Section 1.3.1) use diffusing computations for purposes other than updating least costs (e.g., rollback to a checkpoint in the case of CPR and remove  $\bar{v}$  as a destination during preprocessing). Like DUAL, the purpose of PURGE’s diffusing computations is to prevent routing loops. However, PURGE’s diffusing computations do not verify that new least costs preserve loop free routing (as with DUAL) but instead globally invalidate false routing state.

Jefferson [32] proposes a solution to synchronize distributed systems called Time Warp. Time Warp is a form of optimistic concurrency control and, as such, occasionally requires rolling back to a checkpoint. Time Warp does so by “unsending” each message sent after the time the checkpoint was taken. With our CPR algorithm, a node does not need to explicitly “unsend” messages after rolling back. Instead, each node sends its  $\overrightarrow{min}$  taken at the time of the snapshot, which implicitly undoes the effects of any messages sent after the snapshot timestamp.

## 1.7 Conclusions

In this chapter, we developed methods for recovery in scenarios where a malicious node injects false state into a distributed system. We studied an instance of this problem in distance vector routing. We presented and evaluated three new algorithms for recovery in such scenarios. Among our three algorithms, our results show that CPR – a checkpoint-rollback based algorithm – yields the lowest message and time overhead over topologies with fixed link costs. However, CPR has storage overhead and requires loosely synchronized clocks. In the case of topologies with changing link costs, PURGE performs best by avoiding the problems that plague CPR and 2ND-BEST. Unlike CPR, PURGE has no stale state to update because PURGE does not rollback in time. The count-to-infinity problem results in high message overhead for

2ND-BEST, while PURGE eliminates the count-to-infinity problem by globally purging false state before finding new least cost paths.



## CHAPTER 2

# PMU SENSOR PLACEMENT FOR MEASUREMENT ERROR DETECTION IN THE SMART GRID

### 2.1 Introduction

This chapter considers placing electric power grid sensors, called phasor measurement units (PMUs), to enable measurement error detection. Significant investments have been made to deploy PMUs on electric power grids worldwide. PMUs provide *synchronized* voltage and current measurements at a sampling rate orders of magnitude higher than the status quo: 10 to 60 samples per second rather than one sample every 1 to 4 seconds. This allows system operators to directly measure the state of the electric power grid in real-time, rather than relying on imprecise state estimation. Consequently, PMUs have the potential to enable an entirely new set of applications for the power grid: protection and control during abnormal conditions, real-time distributed control, postmortem analysis of system faults, advanced state estimators for system monitoring, and the reliable integration of renewable energy resources [12].

An electric power system consists of a set of buses – electric substations, power generation centers, or aggregation points of electrical loads – and transmission lines connecting those buses. The state of a power system is defined by the voltage phasor – the magnitude and phase angle of electrical sine waves – of all system buses and the current phasor of all transmission lines. PMUs placed on buses provide real-time measurements of these system variables. However, because PMUs are expensive, they cannot be deployed on all system buses [8][19]. Fortunately, the voltage phasor at a system bus can, at times, be determined (termed *observed* in this paper) even

when a PMU is not placed at that bus, by applying Ohm’s and Kirchhoff’s laws on the measurements taken by a PMU placed at some nearby system bus [8][13]. Specifically, with correct placement of enough PMUs at a subset of system buses, the entire system state can be determined.

In this chapter, we study two sets of PMU placement problems. The first problem set consists of FULLOBSERVE and MAXOBSERVE, and considers maximizing the observability of the network via PMU placement. FULLOBSERVE considers the minimum number of PMUs needed to observe all system buses, while MAXOBSERVE considers the maximum number of buses that can be observed with a given number of PMUs. A bus is said to be *observed* if there is a PMU placed at it or if its voltage phasor can be calculated using Ohm’s or Kirchhoff’s Law. Although FULLOBSERVE is well studied [8, 13, 30, 38, 48], existing work considers only networks consisting solely of zero-injection buses, an unrealistic assumption in practice, while we generalize the problem formulation to include mixtures of zero and non-zero-injection buses. Additionally, our approach for analyzing FULLOBSERVE provides the foundation with which to present the other three new (but related) PMU placement problems.

The second set of placement problems considers PMU placements that support PMU error detection. PMU measurement errors have been recorded in actual systems [46]. One method of detecting these errors is to deploy PMUs “near” each other, thus enabling them to *cross-validate* each-other’s measurements. FULLOBSERVE-XV aims to minimize the number of PMUs needed to observe all buses while insuring PMU cross-validation, and MAXOBSERVE-XV computes the maximum number of observed buses for a given number of PMUs, while insuring PMU cross-validation.

We make the following contributions in this chapter:

- We formulate two PMU placement problems, which (broadly) aim at maximizing observed buses while minimizing the number of PMUs used. Our formula-

tion extends previously studied systems by considering both zero and non-zero-injection buses.

- We formally define graph-theoretic rules for PMU cross-validation. Using these rules, we formulate two additional PMU placement problems that seek to maximize the number of observed buses while minimizing the number of PMUs used under the condition that the PMUs are cross-validated.
- We prove that all four PMU placement problems are NP-Complete. This represents our most important contribution.
- Given the proven complexity of these problems, we evaluate heuristic approaches for solving these problems. For each problem, we describe a greedy algorithm, and prove that each greedy algorithm has polynomial running time.
- Using simulations, we evaluate the performance of our greedy approximation algorithms over synthetic and actual IEEE bus systems. We find that the greedy algorithms yield a PMU placement that is, on average, within 97% optimal. Additionally, we find that the cross-validation constraints have limited effects on observability: on average our greedy algorithm that places PMUs according to the cross-validation rules observes only 5.7% fewer nodes than the same algorithm that does not consider cross-validation.

The rest of this chapter is organized as follows. In Section 2.2 we introduce our modeling assumptions, notation, and observability and cross-validation rules. In Section 2.3 we formulate and prove the complexity of our four PMU placement problems. Section 2.4 presents the approximation algorithms for each problem and Section 2.5 considers our simulation-based evaluation. We conclude with a review of related work (Section 2.6) and concluding remarks (Section 2.7).

## 2.2 Preliminaries

In this section we introduce notation and underlying assumptions (Section 2.2.1), and define our observability (Section 2.2.2) and cross-validation (Section 2.2.3) rules.

### 2.2.1 Assumptions, Notation, and Terminology

We model a power grid as an undirected graph  $G = (V, E)$ . Each  $v \in V$  represents a bus.  $V = V_Z \cup V_I$ , where  $V_Z$  is the set of all zero-injection buses and  $V_I$  is the set of all non-zero-injection buses. A bus is zero-injection if it has no load nor generator [51]. All other buses are non-zero-injection, which we refer to as injection buses. Each  $(u, v) \in E$  is a transmission line connecting buses  $u$  and  $v$ .

Consistent with the conventions in [8, 13, 16, 38, 48, 49], we assume: PMUs can only be placed on buses and a PMU on a bus measures the voltage phasor at the bus and the current phasor of all transmission lines connected to it. For convenience, we refer to any bus with a PMU as a *PMU node*.

For  $v \in V$  define let  $\Gamma(v)$  be the set of  $v$ 's neighbors in  $G$ . A PMU placement  $\Phi_G \subseteq V$  is a set of nodes at which PMUs are placed, and  $\Phi_G^R \subseteq V$  is the set of observed nodes for graph  $G$  with placement  $\Phi_G$  (see definition of observability below).  $k^* = \min\{|\Phi_G| : \Phi_G^R = V\}$  denotes the minimum number of PMUs needed to observe the entire network.

For convenience, we refer to any node with a PMU as a *PMU node*. Additionally, for a given PMU placement we shall say that a set  $W \subseteq V$  is observed if all nodes in the set are observed, and if  $W = V$  we refer to the graph as *fully observed*.

### 2.2.2 Observability Rules

We use the simplified observability rules stated by Brueni and Heath [13]:

1. **Observability Rule 1 (O1).** *If node  $v$  is a PMU node, then  $v \cup \Gamma(v)$  is observed.*

2. **Observability Rule 2 (O2).** *If a zero-injection node,  $v$ , is observed and  $\Gamma(v) \setminus \{u\}$  is observed for some  $u \in \Gamma(v)$ , then  $v \cup \Gamma(v)$  is observed.*

Since O2 only applies with zero-injection nodes, the number of zero-injection nodes can greatly affect system observability.

### 2.2.3 Cross-Validation Rules

Cross-validation formalizes the intuitive notion of placing PMUs “near” each other to allow for measurement error detection. For convenience, we say a PMU is cross-validated even though it is actually the PMU data at a node that is cross-validated. A PMU is *cross-validated* if one of the rules below is satisfied [46]:

1. **Cross-Validation Rule 1 (XV1).** *If two PMU nodes are adjacent, then the PMUs cross-validate each other.*
2. **Cross-Validation Rule 2 (XV2).** *If two PMU nodes have a common neighbor, then the PMUs cross-validate each other.*

XV1 derives from the fact that both PMUs are measuring the current phasor of the transmission line connecting the two PMU nodes. XV2 is more subtle. Using the notation specified in XV2, when computing the voltage phasor of an element in  $\Gamma(u) \cap \Gamma(v)$  the voltage equations include variables to account for measurement error (e.g., angle bias) [45]. When the PMUs are two hops from each other (i.e., have a common neighbor), there are more equations than unknowns, allowing for measurement error detection. Otherwise, the number of unknown variables exceeds the number of equations, which eliminates the possibility of detecting measurement errors [45].

## 2.3 Four NP-Complete PMU Placement Problems

In this section we define four PMU placement problems (FULLOBSERVE, MAXOBSERVE, FULLOBSERVE-XV, and MAXOBSERVE-XV) and prove their NP-Completeness.

FULLOBSERVE-XV and MAXOBSERVE-XV both consider measurement error detection, while FULLOBSERVE and MAXOBSERVE do not. In effort to keep this proposal document relatively short, we omit the actual NP-Completeness proofs and instead present proof sketches; details can be found in [27]. We begin this section with a high-level description of the proof strategy we use to prove each problem is NP-Complete (Section 2.3.1). In Section 2.3.2, we state our four PMU placement problems and outline our NP-Completeness proofs for each.

### 2.3.1 Overview of NPC Proof Strategy

In this section, we outline the proof strategy we use in each of our NP-Completeness proofs. Our proofs follow a similar structure to those proposed by Brueni and Heath [13]. The authors prove NP-Completeness by reduction from planar 3-SAT (P3SAT). A 3-SAT formula,  $\phi$ , is a boolean formula in conjunctive normal form (CNF) such that each clause contains at most 3 literals. For any 3-SAT formula  $\phi$  with the sets of variables  $\{v_1, v_2, \dots, v_r\}$  and clauses  $\{c_1, c_2, \dots, c_s\}$ ,  $G(\phi)$  is the bipartite graph  $G(\phi) = (V(\phi), E(\phi))$  defined as follows:

$$\begin{aligned} V(\phi) &= \{v_i \mid 1 \leq i \leq r\} \cup \{c_j \mid 1 \leq j \leq s\} \\ E(\phi) &= \{(v_i, c_j) \mid v_i \in c_j \text{ or } \overline{v_i} \in c_j\}. \end{aligned}$$

Note that edges pass only between  $v_i$  and  $c_j$  nodes, and so the graph is bipartite. P3SAT is a 3-SAT formula such that  $G(\phi)$  is planar [34]. For example, P3SAT formula

$$\begin{aligned} \varphi &= (\overline{v_1} \vee v_2 \vee v_3) \wedge (\overline{v_1} \vee \overline{v_4} \vee v_5) \wedge (\overline{v_2} \vee \overline{v_3} \vee \overline{v_5}) \\ &\quad \wedge (v_3 \vee \overline{v_4}) \wedge (\overline{v_3} \vee v_4 \vee \overline{v_5}) \end{aligned} \tag{2.1}$$

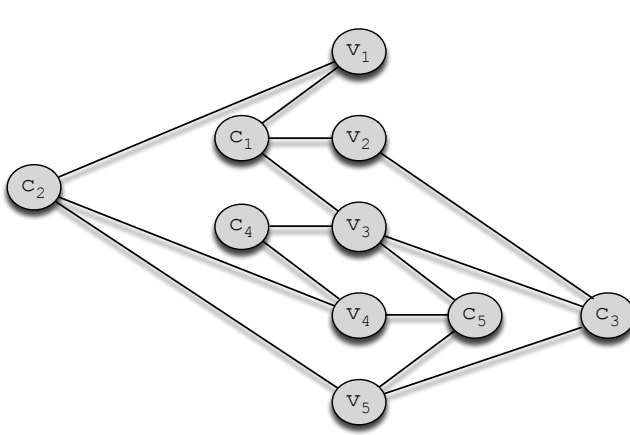
has graph  $G(\varphi)$  shown in Figure 2.1(a). Discovering a satisfying assignment for P3SAT is an NPC problem, and so it can be used in a reduction to prove the complexity of the problems we address here.

Following the approach in [13], for P3SAT formula,  $\phi$ , we replace each variable node and each clause node in  $G(\phi)$  with a specially constructed set of nodes, termed a *gadget*. In this work, all variable gadgets will have the same structure, and all clause gadgets have the same structure (that is different from the variable gadget structure), and we denote the resulting graph as  $H(\phi)$ . In  $H(\phi)$ , each *variable* gadget has a subset of nodes that semantically represent assigning “True” to that variable, and a subset of nodes that represent assigning it “False”. When a PMU is placed at one of these nodes, this is interpreted as assigning a truth value to the P3SAT variable corresponding with that gadget. Thus, we use the PMU placement to determine a consistent truth value for each P3SAT variable. Also, clause gadgets are connected to variable gadgets at either “True” or “False” (but never both) nodes, in such a way that the clause is satisfied if and only if *at least one* of those nodes has a PMU.

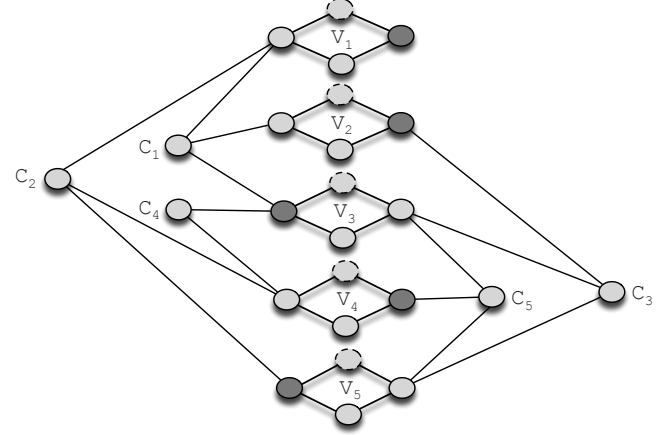
While we assume  $G(\phi)$  is planar, we make no such claim regarding  $H(\phi)$ , though in practice all graphs used in our proofs are indeed planar. The proof of NPC rests on the fact that solving the underlying  $\phi$  formula is NPC.

In what follows, for a given PMU placement problem  $\Pi$ , we prove  $\Pi$  is NPC by showing that a PMU placement in  $H(\phi)$ ,  $\Phi$ , can be interpreted semantically as describing a satisfying assignment for  $\phi$  iff  $\Phi \in \Pi$ . Since P3SAT is NPC, this proves  $\Pi$  is NPC as well.

While the structure of our proofs is adapted from [13], the variable and clause gadgets we use to correspond to the P3SAT formula are novel, thus leading to a different set of proofs. Our work here demonstrates how the work in [13] can be extended, using new variable and clause gadgets, to address a wide array of PMU placement problems.



(a)  $G(\varphi)$  formed from  $\varphi$  in Equation (2.1).



(b) Graph formed from  $\varphi$  formula in Theorem 2.1 proof.

**Figure 2.1.** The figure in (a) shows  $G(\varphi) = (V(\varphi), E(\varphi))$  using example formula,  $\varphi$ , from Equation (2.1). (b) shows the new graph formed by replacing each variable node in  $G(\varphi)$  – as specified by the Theorem 2.1 proof – with the Figure 2.2(a) variable gadget.

### 2.3.2 Problem Statements and NPC Proof Sketches

Here we briefly define each of our four PMU placement problems: FULLOBSERVE, MAXOBSERVE, MAXOBSERVE-XV, and FULLOBSERVE-XV. Then, we provide proof sketches (that follow the proof strategy outlined in the previous section) demonstrating that each algorithm is NP-Complete.

#### FullObserve Decision Problem:

Instance: Graph  $G = (V, E)$  where  $V = V_Z \cup V_I$ ,  $V_Z \neq \emptyset$ ,  $k$  PMUs such that  $k \geq 1$ .

Question: Is there a  $\Phi_G$  such that  $|\Phi_G| \leq k$  and  $\Phi_G^R = V$ ?

**Theorem 2.1.** FULLOBSERVE is NP-Complete.

*Proof Sketch:* We introduce a problem-specific variable gadget shown in Figure 2.2(a) and a single node as the clause gadget. We show that in order to observe all nodes, PMUs must be placed on variable gadgets, specifically on nodes that semantically correspond to True and False values that satisfy the corresponding P3SAT formula.



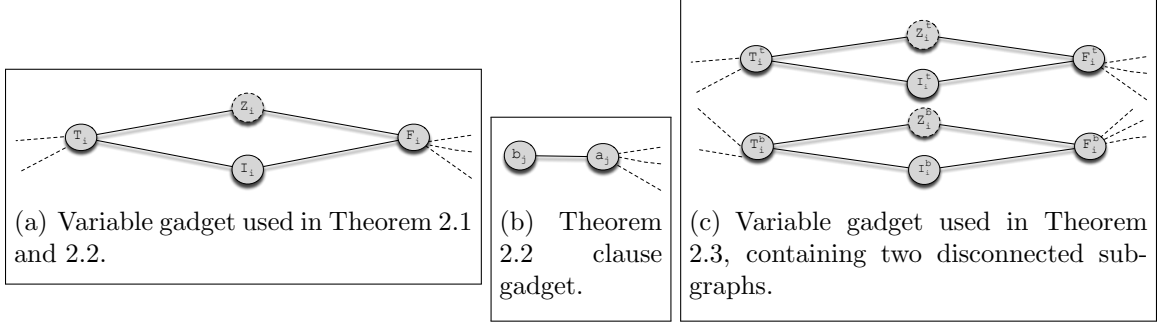


**Figure 2.2.** Gadgets used in Theorem 2.1 - 2.4.  $Z_i$  in Figure 2.2(a),  $Z_i^t$  in Figure 2.2(c), and  $Z_i^b$  in Figure 2.2(c) are the only zero-injection nodes. The dashed edges in Figure 2.2(a) and Figure 2.2(c) are connections to clause gadgets. Likewise, the dashed edges in Figure (b) are connections to variable gadgets. In Figure 2.2(c), superscript,  $t$ , denotes nodes in the upper subgraph and superscript,  $b$ , indexes nodes in the lower subgraph.

Consider the example P3SAT formula from Equation 2.1,  $\varphi$ , and its corresponding bipartite graph,  $G(\varphi)$ , shown in Figure 2.1(a). Our proof procedure replaces each variable node in  $G(\varphi)$  with the variable gadget shown in Figure 2.2(a), yielding the graph shown in Figure 2.1(b). Nodes with a dashed border are zero-injection nodes.  $\varphi$  is satisfied when literals  $\overline{v_1}$ ,  $\overline{v_2}$ ,  $v_3$ ,  $\overline{v_4}$ , and  $\overline{v_5}$  are all True, yielding a PMU placement with PMUs at each dark shaded node in Figure 2.1(b).

### MaxObserve Decision Problem:

Instance: Graph  $G = (V, E)$  where  $V = V_Z \cup V_I$ ,  $k$  PMUs such that  $1 \leq k < k^*$ .

Question: For a given  $m < |V|$ , is there a  $\Phi_G$  such that  $|\Phi_G| \leq k$  and  $m \leq |\Phi_G^R| < |V|$ ?

**Theorem 2.2.** MAXOBSERVE is NP-Complete.

*Proof Sketch:* First, we construct problem-specific gadgets for variables (Figure 2.2(a)) and clauses (Figure 2.2(b)). We then demonstrate that any solution that observes  $m$  nodes must place the PMUs only on nodes in the variable gadgets. Next we show that as a result of this, the problem of observing  $m$  nodes in this graph reduces to Theorem 2.1.

**FullObserve-XV Decision Problem:**

Instance: Graph  $G = (V, E)$  where  $V = V_Z \cup V_I$ ,  $k$  PMUs such that  $k \geq 1$ .

Question: Is there a  $\Phi_G$  such that  $|\Phi_G| \leq k$  and  $\Phi_G^R = V$  under the condition that each  $v \in \Phi_G$  is cross-validated?

**Theorem 2.3.** FULLOBSERVE-XV is NP-Complete.

*Proof Sketch:* We show FULLOBSERVE-XV is NP-hard by reducing from P3SAT. We create a single-node gadget for clauses (as we did with FULLOBSERVE) and the gadget shown in Figure 2.2(c) for each variable. Each variable gadget here comprises of two disconnected components, and there are two  $T_i$  and two  $F_i$  nodes, one in each component. First, we show that each variable gadget must have 2 PMUs for the entire graph to be observed, one PMU for each subgraph. Then, we show that cross-validation constraints force PMUs to be placed on both  $T$  nodes or both  $F$  nodes. Finally, we use the PMU placement to derive a satisfying P3SAT truth assignment.

**MaxObserve-XV Decision Problem:**

Instance: Graph  $G = (V, E)$  where  $V = V_Z \cup V_I$ ,  $k$  PMUs such that  $1 \leq k < k^*$ , and some  $m < |V|$ .

Question: Is there a  $\Phi_G$  such that  $|\Phi_G| \leq k$  and  $m \leq |\Phi_G^R| < |V|$  under the condition that each  $v \in \Phi_G$  is cross-validated?

**Theorem 2.4.** MAXOBSERVE-XV is NP-Complete.

*Proof Sketch:* Our proof is a combination of the NP-Completeness proofs for MAXOBSERVE and FULLOBSERVE-XV.

## 2.4 Approximation Algorithms

Because all four placement problems are NPC, we propose greedy approximation algorithms for each problem, which iteratively add a PMU in each step to the node that observes the maximum number of new nodes. We present two such algorithms,

one that directly addresses MAXOBSERVE (**greedy**) and the other MAXOBSERVE-XV (**xvgreedy**). **greedy** and **xvgreedy** can easily be used to solve FULLOBSERVE and FULLOBSERVE-XV, respectively, by selecting the appropriate  $k$  value to ensure full observability.

**greedy Algorithm.** We start with  $\Phi = \emptyset$ . At each iteration, we add a PMU to the node that results in the observation of the maximum number of new nodes. The algorithm terminates when all PMUs are placed.<sup>1</sup>

**xvgreedy Algorithm.** **xvgreedy** is almost identical to **greedy**, except that PMUs are added in pairs such that the selected pair observe the maximum number of nodes under the condition that the PMU pair satisfy one of the cross-validation rules.

## 2.5 Simulation Study

**Topologies.** We evaluate our approximation algorithms with simulations over synthetic topologies generated using real portions of the North American electric power grid (i.e., IEEE bus systems 14, 30, 57, and 118) as templates<sup>2</sup>. The bus system number indicates the number of nodes in the graph (e.g., bus system 57 has 57 nodes). It is standard practice in the literature to only use single IEEE bus systems [8, 16, 38, 48]. We follow this precedent but do not present these results because they are consistent with the trends found using synthetic topologies. Instead, we focus on synthetic topologies because, unlike simulations using single IEEE bus systems, we can establish the statistical significance of the performance of our greedy approximations.

Since observability is determined by the connectivity of the graph, we use the *degree distribution* of IEEE topologies as the template for generating our synthetic

---

<sup>1</sup>The same greedy algorithm is proposed by Aazami and Stilp [4].

<sup>2</sup><http://www.ee.washington.edu/research/pstca/>

graphs. A synthetic topology is generated from a given IEEE graph by randomly “swapping” edges in the IEEE graph. Specifically, we select a random  $v \in V$  and then pick a random  $u \in \Gamma(v)$ . Let  $u$  have degree  $d_u$ . Next, we select a random  $w \notin \Gamma(v)$  with degree  $d_w = d_u - 1$ . Finally, we remove edge  $(v, u)$  and add  $(v, w)$ , thereby preserving the node degree distribution. We continue this swapping procedure until the original graph and generated graph share *no edges*, and then return the resulting graph.

**Evaluation Methods.** We are interested in evaluating how close our algorithms are to the optimal PMU placement. Thus, when computationally possible (for a given  $k$ ) we use brute-force algorithms to iterate over all possible placements of  $k$  PMUs in a given graph and select the best PMU placement. When the brute-force algorithm is computationally infeasible, we present only the performance of the greedy algorithm. In what follows, the output of the brute-force algorithm is denoted `optimal`, and when we require cross-validation it is denoted `xvoptimal`.

**Simulation Results.** We vary the number of PMUs and determine the number of observed nodes in the synthetic graph. Each data point is generated as follows. For a given number of PMUs,  $k$ , we generate a graph, place  $k$  PMUs on the graph, and then determine the number of observed nodes. We continue this procedure until  $[0.9(\bar{x}), 1.1(\bar{x})]$  – where  $\bar{x}$  is the mean number of observed nodes using  $k$  PMUs – falls within the 90% confidence interval.

In addition to generating a topology, for each synthetic graph we determined the members of  $V_I, V_Z$ . These nodes are specified for the original graphs in the IEEE bus system database. Thus, we randomly map each node in the IEEE graph to a node in the synthetic graph with the same degree, and then match their membership to either  $V_I$  or  $V_Z$ .

Due to space constraints, we only show plots for solving MAXOBSERVE and MAXOBSERVE-XV using synthetic graphs based on IEEE bus 57. The number of

nodes observed given  $k$ , using **greedy** and **optimal**, are shown in Figure 2.3(a), and Figure 2.3(b) shows this number for **xvgreedy** and **xvoptimal**. Both plots include the 90% confidence intervals. Results for synthetic graphs generated using IEEE bus 14, 30, and 118 yield the same trends.

Our greedy algorithms perform well. On average, **greedy** is within 98.6% of **optimal**, is never below 94% of **optimal**, and in most cases gives the optimal result. Likewise, **xvgreedy** is never less than 94% of **xvoptimal** and on average is within 97% of **xvoptimal**. In about half the cases **xvgreedy** gives the optimal result. These results suggest that despite the complexity of the problems, a greedy approach can return high-quality results. Note, however, that these statistics do not include performance when  $k$  is large. It is an open question whether **greedy** and **xvgreedy** would do well for large  $k$ .

Surprisingly, when comparing our results with and without the cross-validation requirement, we find that the cross-validation constraints have little effect on the number of observed nodes for the same  $k$ . Our experiments show that on average **xvoptimal** observed only 5% fewer nodes than **optimal**. Similarly, on average **xvgreedy** observes 5.7% fewer nodes than **greedy**. This suggests that the cost of imposing the cross-validation requirement is low, with the clear gain of ensuring PMU correctness across the network.

## 2.6 Related Work

FULLOBSERVE is well-studied [8, 13, 30, 38, 48]. Haynes et al. [30] and Brueni and Heath [13] both prove FULLOBSERVE is NPC. However, their proofs make the unrealistic assumption that all nodes are zero-injection. We drop this assumption and thereby generalize their NPC results for FULLOBSERVE. Additionally, we leverage the proof technique from Brueni and Heath [13] in all four of our NPC proofs, although our proofs differ considerably in their details.

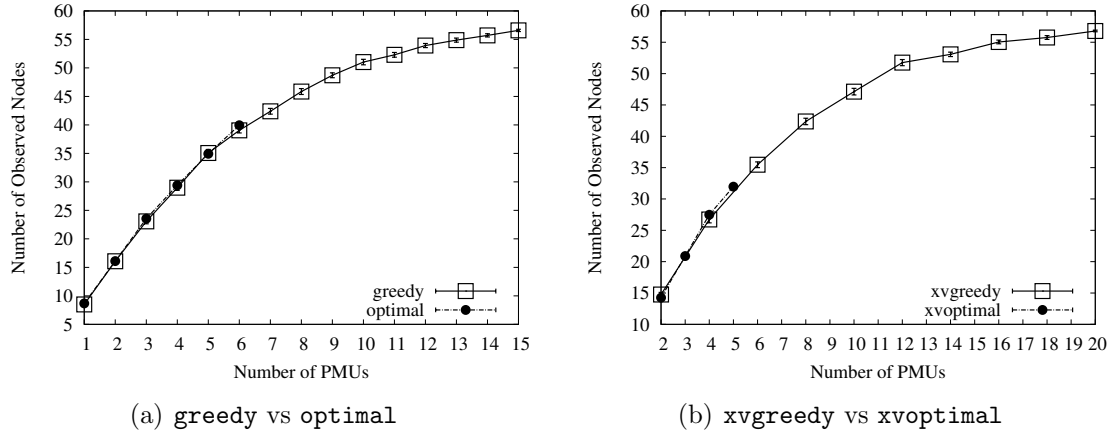


**Figure 2.3.** Mean number of observed nodes over synthetic graphs based on IEEE bus 57 when varying number of PMUs. The 90% confidence interval is shown.

In the power systems literature, Xu and Abur [48, 49] use integer programming to solve FULLOBSERVE, while Baldwin et al. [8] and Mili et al. [38] use simulated annealing to solve the same problem. All of these works allow nodes to be either zero-injection or non-zero-injection. However, these chapter papers make no mention that FULLOBSERVE is NPC, i.e., they do not characterize the fundamental complexity of the problem.

Aazami and Stilp [4] investigate approximation algorithms for FULLOBSERVE. They derive a hardness approximation threshold of  $2^{\log^{1-\epsilon} n}$ . Also they prove that in the worst case, **greedy** from Section 2.4 does no better  $\Theta(n)$  of the optimal solution. However, this approximation ratio assumes that all nodes are zero-injection.

Chen and Abur [16] and Vanfretti et al. [46] both study the problem of bad PMU data. Chen and Abur [16] formulate their problem differently than FULLOBSERVE-XV and MAXOBSERVE-XV. They consider fully observed graphs and add PMUs to the system to make all existing PMU measurements non-critical (a critical measurement is one in which the removal of a PMU makes the system no longer fully observable). Vanfretti et al. [46] define the cross-validation rules used in this chapter.

They also derive a lower bound on the number of PMUs needed to ensure all PMUs are cross-validated and the system is fully observable.

## 2.7 Conclusions

In this chapter, we formulated four PMU placement problems and proved that each one is NPC. Consequently, future work should focus on developing approximation algorithms for these problems. As a first step, we presented two simple greedy algorithms: **xvgreedy** which considers cross-validation and **greedy** which does not. Both algorithms iteratively add PMUs to the node which observes the maximum of number of nodes.

Using simulations, we found that our greedy algorithms consistently reached close-to-optimal performance. We also found that cross-validation had a limited effect on observability: for a fixed number of PMUs, **xvgreedy** and **xvoptimal** observed only 5% fewer nodes than **greedy** and **optimal**, respectively. As a result, we believe imposing the cross-validation requirement on PMU placements is advised, as the benefits they provide come at a low marginal cost.

## CHAPTER 3

# RECOVERY FROM LINK FAILURES IN A SMART GRID COMMUNICATION NETWORK

### 3.1 Introduction

An electric power grid consists of a set of buses – electric substations, power generation centers, or aggregation points of electrical loads – and transmission lines connecting those buses. The operation of the power grid can be greatly improved by high-frequency voltage and current measurements. Phasor Measurement Units (PMUs) are sensors that provide such measurements. PMUs are currently being deployed in electric power grids worldwide, providing the potential to both (a) drastically improve existing power grid operations and applications and (b) enable an entirely new set of applications, such as real-time visualization of electric power grid dynamics and the reliable integration of renewable energy resources.

PMU applications have stringent and in many cases ultra-low *per-packet* delay and loss requirements. If these per-packet delay requirements are not met, PMU applications can miss a critical power grid event (e.g., lightning strike, power link failure), potentially leading to a cascade of incorrect decisions and corresponding actions. For example, closed-loop control applications require delays of 8 – 16 ms per-packet [7]. If *any* packet is not received within this time window, the closed-loop control application may take a wrong control action. In the worst case, this can lead to a cascade of power grid failures (e.g., the August 2003 blackout in the USA <sup>1</sup> and the recent power grid failures in India [50]).

---

<sup>1</sup>[http://en.wikipedia.org/wiki/Northeast\\_blackout\\_of\\_2003](http://en.wikipedia.org/wiki/Northeast_blackout_of_2003)



As a result of this sensitivity, the communication network that disseminates PMU data must provide hard end-to-end data delivery guarantees [7]. For this reason, the Internet’s best-effort service model alone is unable to meet the stringent packet delay and loss requirements of PMU applications [11]. Instead, either a new network architecture or enhancements to Internet architecture and protocols are needed [7, 11, 12, 31] to provide efficient, in-network forwarding and fast recovery from link and switch failures. Additionally, multicast should figure prominently in data delivery, since PMUs disseminate data to applications across many locations [7].

In this last piece of our research, we design algorithms for fast recovery from link failures in a Smart Grid communication network. Informally, we consider a link that does not meet its packet delivery requirement (either due to excessive delay or actual packet loss) as failed. Our proposed research divides broadly into two parts:

- **Link detection failure.** Here, we design link-failure detection and reporting mechanisms that use OpenFlow [36] – an open source framework that centralizes network management and control – to detect link failures when and where they occur, *inside* the network. In-network detection is used to reduce the time between when the loss occurs and when it is detected. In contrast, most previous work [5, 14, 25] focuses on measuring end-to-end packet loss, resulting in slower detection times.
- **Algorithms for pre-computing backup multicast trees.** Inspired by MPLS fast-reroute algorithms that are used in practice to quickly reroute time-critical unicast IP flows over pre-computed backup paths [18, 23, 37, 42, 47], we propose a set of algorithms, each of which computes backup multicast trees that are installed after a link failure. We also implement these algorithms in OpenFlow and demonstrate their performance.

Each algorithm computes backup multicast trees that aim to minimize end-to-end packet loss and delay, but each algorithm uses different optimization criteria in achieving this goal: minimizing control overhead (MIN-CONTROL), minimizing the number of affected flows across all multicast trees (MIN-FLOWS), and minimizing the number of affected sink nodes across all multicast trees (MIN-SINKS). These optimization criteria differ from those proposed in the literature. For example, most previous work [18, 23, 37, 42, 47] uses optimization criteria specified over a *single* multicast tree, while we must consider criteria specified across *multiple* multicast trees. Finally, because the smart grid network is many orders of magnitudes smaller than the Internet <sup>2</sup> and multicast group membership is mostly static in the Smart Grid, we can for the most part avoid the scalability issues of Internet-based solutions [18, 23, 37, 42, 47].

The remainder of this chapter is structured as follows. In the following section 3.2, we briefly survey relevant literature. We outline proposed research in Section 3.3: section 3.3.3 details our research thus far on link-failure detection in OpenFlow, and in section 3.3.5, we outline our algorithms for computing backup multicast trees. Our treatment here is necessarily brief, but we indicate work completed thus far as well as proposed future work. Section 3.4 concludes this chapter with a summary of our proposed research and timeline for future work.

## 3.2 Background and Related Work

### 3.2.1 PMU Applications and Their QoS Requirements

The QoS requirements of several PMU applications planned to be deployed on power grids worldwide are presented in Table 3.1, based on [7, 17]. We refer the reader to the actual documents for a description of each PMU application. The end-

---

<sup>2</sup>For example, it is estimated that fewer than  $10^4$  routers/switches are needed for a smart grid network spanning the *entire* USA, whereas there are about  $10^8$  routers in the Internet [7].

PMU Application	E2E Delay	Rate (Hz)	NASPI Class
♡ Oscillation Detection	0.25 – 3 secs	10 – 50	N/A
♡ Frequency Instability	0.25 – 0.5 secs	1 – 50	N/A
♡ Voltage Instability	1 – 2 secs	1 – 50	N/A
♡ Line Temp. Monitoring	5 minutes	1	N/A
△ Closed-Loop Control	8 – 16 ms	120 – 720+	A
△ Direct State Measurement	5 – 1000+ ms	1 – 720+	B
△ Operator Displays	1000+ ms	1 – 120	D
△ Distributed Wide Area Control	1 – 240 ms	1 – 240	B
△ System Protection	5 – 50 ms	120 – 720+	A
△ Anti-Islanding	5 – 50 ms	30 – 720+	A
△ Post Event Analysis	1000+ ms	< 1	E

**Table 3.1.** PMU applications and their QoS requirements. The ♡ refers to reference [17] and △ to [7].

to-end (E2E) delay requirement is at the *per-packet* level, as advocated by Bakken et al. [7].

NASPI defines five service classes (A-E) for Smart Grid traffic, each designating qualitative requirements for latency, availability, accuracy, time alignment, message rate, and path redundancy [7]. At one end of the spectrum, service class A applications have the most stringent requirements, while service Class E designates applications with the least demanding requirements.

In this work, we focus on PMU applications with the most stringent E2E delay requirements, such as closed-loop control and system protection. In particular, we create a binary classification of data plane traffic: traffic belonging to critical PMU applications and all other traffic.

### 3.2.2 OpenFlow

OpenFlow is an open source framework that cleanly separates the control and data planes, and provides a programmable (and possibly centralized) control framework [36]. All OpenFlow algorithms and protocols are managed by a (logically) centralized controller, while network switches/routers (as their only task) forward packets ac-

cording to the flow tables installed by the controller. By allowing a more centralized network control and management framework, the OpenFlow architecture avoids the high storage, computation, and management overhead that plague many distributed network approaches. Our multicast tree repair algorithms benefit from these OpenFlow features (Section 3.3.5).

OpenFlow exposes the flow tables of its switches, allowing the controller to add, remove, and delete flow entries, which determine how switches forward, copy, or drop packets associated with a controller-managed flow. Phrased differently, OpenFlow switches follow a “match and action” paradigm [36], in which each switch *matches* an incoming packet to a flow table table entry and then takes some *action* (e.g., forwards, drops, or copies the packet). Each switch also maintains per-flow statistics (e.g., packet counter, number of bytes received, time the flow was installed) that can be queried by the controller. In summary, OpenFlow provides a flexible framework for *in-network* packet loss detection as demonstrated by our detection algorithms (Section 3.3.3).

### 3.2.3 Related Work

#### 3.2.3.1 Smart Grid Communication

The Gridstat project <sup>3</sup>, started in 1999, was one of the first research projects to consider smart grid communication. Our work has benefited from their detailed requirements specification [7].

Gridstat proposes a publish-subscribe architecture for PMU data dissemination. By design, subscription criteria are simple to enable fast forwarding of PMU data (and as a measure towards meeting the low latency requirements of PMU applications). Gridstat separates their system into a data plane and a management plane. The management plane keeps track of subscriptions, monitors the quality of service provided

---

<sup>3</sup><http://gridstat.net/>

by the data plane, and computes paths from subscribers to publishers. To increase reliability, each Gridstat publisher sends data over multiple paths to each subscriber. Each of these paths is a part of a different (edge-disjoint) multicast tree. Meanwhile, the data plane simply forwards data according to the paths and subscription criteria maintained by the management plane.

Although Gridstat has similarities with our work, their project lacks details. For example, no protocol is provided defining communication between the management and data plane. Additionally, there is no explicit indication if the multicast trees are source-based.

In North America, all PMU deployments are overseen by the North American SynchroPhasor Initiative (NASPI) [12]. NASPI has proposed and started (as of December 2012) to build the communication network used to deliver PMU data, called NASPInet. The interested reader can consult [12] for more details.

Hopkinson et al [31] propose a Smart Grid communication architecture that handles heterogeneous traffic: traffic with strict timing requirements (e.g., protection systems), periodic traffic with greater tolerance for delay, and aperiodic traffic. They advocate a multi-tier data dissemination architecture: use a technology such as MPLS to make hard bandwidth reservations for critical applications, use Gridstat to handle predictable traffic with less strict delivery requirements, and finally use Astrolab (which uses a gossip protocol) to manage aperiodic traffic sent over the remaining available bandwidth. They advocate hard bandwidth reservations – modeled as a multi-commodity flow problem – for critical Smart Grid applications.

### **3.2.3.2 Detecting Packet Loss**

Most previous work [5, 14, 25] focuses on measuring and detecting packet loss on an end-to-end packet basis. Because PMU applications have small per-packet delay requirements (Section 3.2.1), the time delay between when the loss occurs and

when it is detected needs to be small. For this reason, we will investigate detecting lossy links *inside* the network. Additionally, most previous work takes an *active measurement* approach towards detecting lossy links in which probe messages are injected to estimate packet loss. Injecting packets can potentially skew measurements – especially since accurate packet loss estimates require a high sampling probing rate – leading to inaccurate results [9].

Friedl et al. [25] propose a *passive* measurement algorithm that directly measures actual network traffic to determine application-level packet loss rates. Unfortunately, their approach can only measure packet loss after a flow is expired. This makes their algorithm unsuitable for our purposes because PMU application flows are long lasting (running continuously for days, weeks, and even years). For this reason we propose a new algorithm, FAILED-LINK, that provides in-network packet loss detection for long running active flows (Section 3.3.3).

We note that existing Internet routing algorithms (e.g., OSPF, ISIS, BGP) perform in-network detection of link failure, but not of individual packet loss. They do so by having routers exchange “keep-alive” or “hello” messages and detect a link failure when these messages or their acknowledgments are lost.

### 3.2.3.3 Multicast Tree Recovery

Approaches to multicast fault recovery can be broadly divided into two groups: on-demand and preplanned. In keeping with their best-effort philosophy, most Internet-based algorithms compute recovery paths on-demand [18]. Because the Smart Grid is a critical system and its applications have strict delivery requirements, we focus instead on preplanned recovery path computations.

To date, nearly all preplanned approaches [18, 23, 37, 42, 47] are implemented (or suggest an implementation) using virtual circuit packet switching, namely, MPLS. For convenience, in the remainder of this section we assume MPLS is the virtual

circuit packet switching technology used, realizing that other such technologies could be used in its place.

Cui et al [18] define four categories for preplanned multicast path recovery: (a) link protection, (b) path protection, (c) dual-tree protection, and (d) redundant tree protection. With link protection, a backup path is precomputed for each link, connecting the link’s end-nodes [42, 47]. For each destination, a path protection algorithm computes a vertex-disjoint path with the original multicast tree path between the source and destination [47]. The dual-tree approach precomputes a backup tree for each multicast tree. The backup (dual) tree is not required to be node- or link-disjoint with the primary tree but this is desirable [23]. Finally, a redundant tree is node (link) disjoint from the primary tree, thereby ensuring that any destination remains reachable, either by the primary or redundant tree, if any vertex (edge) is eliminated [37].

Distributed multicast recovery schemes, like the ones discussed above, must navigate an inherent trade-off between high overhead and fast recovery (i.e., the time between when the failure is detected and when the multicast tree is repaired is small) [18]. Here, overhead refers to (i) per-router state that needs to be stored and managed and (ii) message complexity. Because preplanned MPLS-based approaches are tailored to support Internet-based applications – typically having a large number of multicast groups and dynamic group membership – scalability is key. Some of the preplanned approaches (dual-tree and redundant trees) focus more on scalability [18, 23, 37], while others (link and path protection schemes) optimize for fast recovery [42, 47].

For two reasons, our algorithms avoid these scalability issues: we use a centralized control architecture (OpenFlow) rather than a distributed one and the Smart Grid operating environment is very different from the Internet-based applications discussed in the literature. Using OpenFlow’s centralized architecture, we store all precomputed

backup/recovery paths at the controller. Thus, we avoid the storage and maintenance issues that distributed approaches must address [18, 23, 42, 47]. In other words, OpenFlow allows our algorithms to bypass the inherent trade-off of high overhead and fast recovery, allowing (for the first time) both fast *and* scalable recovery algorithms.

In the case where the controller is unable to manage router and backup path state, we can simply provision more servers to store precomputed paths. Such a situation is unlikely, considering: the encouraging scalability results reported using a centralized Ethane controller [15] (Ethane is a precursor to OpenFlow that also separates the control and data planes), the Smart Grid is many orders of magnitude smaller than the Internet, and multicast group membership is mostly static in the Smart Grid [7].

Finally, our recovery algorithms use different optimization criteria from previous work considered in this document [18, 23, 37, 42, 47]. Each of these earlier approaches uses optimization criteria specified over a *single* multicast tree, while we must consider criteria specified across *multiple* multicast trees. In addition, none of these approaches explicitly optimize for the criteria we consider: control overhead, number of effected flows, number of affected downstream nodes, and the expected disruption caused by future link failures. Instead, previous work computes backup paths or trees that optimize one of the following criteria: maximize node (link) disjointedness with the primary path [18, 23, 37], minimize bandwidth usage [47], or minimize the number of group members which become disconnected (using either the primary or backup path) after a link failure [42].

### 3.3 Proposed Research

In this section, we present an example problem scenario (Section 3.3.1), which we reference to explain: our link failure detection algorithm (Section 3.3.3), steps to uninstall trees that become disconnected after a link failure (Section 3.3.4), steps



to install backup multicast trees (Section 3.3.4), and our algorithms for computing backup multicast trees (Section 3.3.5).

### 3.3.1 Preliminaries

#### 3.3.1.1 Example Scenario

Figure 3.1 depicts a scenario where a single link,  $(b, c)$ , in a multicast tree fails. Figure 3.1(a) shows a multicast tree rooted at  $a$  with leaf nodes (i.e., data sinks)  $\{e, f, g\}$ .  $a$  sends PMU data at a fixed rate and each data sink specifies a per-packet delay requirement. The multicast tree in Figure 3.1(a) uses link  $(b, c)$ , which we assume fails between the time the snapshots in Figure 3.1(a) and Figure 3.1(b) are taken. When  $(b, c)$  fails, it prevents  $e$  and  $f$  from receiving any packets until the multicast tree is repaired, leaving  $e$  and  $f$ 's per-packet delay requirements unsatisfied. Figure 3.1(b) shows a backup multicast tree installed after  $(b, c)$  fails. Notice that the backup tree does not contain any paths using the failed link,  $(b, c)$ , and has a path between the root ( $a$ ) and each data sink ( $\{e, f, g\}$ ). In the coming sections we present algorithms that allow multicast trees, such as the one shown in Figure 3.1(a), to recover from link failures by installing backup multicast trees, similar to the one in Figure 3.1(b).

#### 3.3.1.2 General Problem Scenario and Basic Notation

Before presenting our algorithms, we first provide a more general problem scenario than the one in Figure 3.1 and introduce some basic notation. We consider a network of nodes modeled as an undirected graph  $G = (V, E)$ . There are three types of nodes: nodes that send PMU data (PMU nodes), nodes that receive PMU data (data sinks), and switches connecting PMU nodes and data sinks (typically via other switches). We assume  $G$  has  $m > 1$  source-based multicast trees to disseminate PMU data. Let  $T = \{T_1, T_2, \dots, T_m\}$ , such that each  $T_i = (V_i, E_i) \in T$  is a source-based multicast tree (MT). We assume  $G$  only contains MTs in  $T$ .

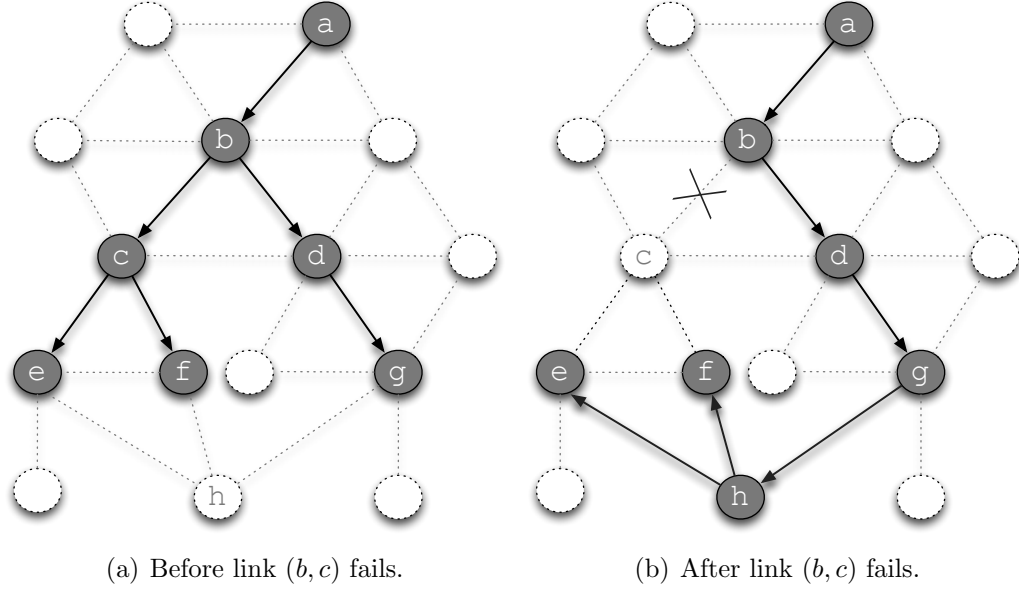


**Figure 3.1.** Example used in Section 3.3.2. The shaded nodes are members of the source-based multicast tree rooted at  $a$ . The lightly shaded nodes are not a part of the multicast tree.

Each PMU node is the source of its own MT and each data sink has a per-packet delay requirement, specified as the maximum tolerable per-packet delay. *Packet delay* between a sender,  $s$ , and receiver,  $r$ , is the time it takes  $s$  to send a packet to  $r$ . We consider any packet received beyond the maximum delay threshold as lost. Note that a data sink's per-packet delay requirement is an end-to-end requirement. Before any link fails, we assume that all PMU data is correctly delivered such that each data sink's per-packet delay requirement is satisfied.

Data sent from a single sender and single data sink is called a *unicast flow*. A unicast flow is uniquely defined by a four-tuple of source address, source port, destination address, and destination port. We assume that data from a single PMU maps to a single port at the source and, likewise, a unique port at the destination.

Because the network supports multicast communication, *multicast flows* (as opposed to unicast flows) are used inside the network. Informally, a multicast flow

contains multiple unicast flows and only sends a single packet across a link. We use notation  $s, \{d_1, d_2, \dots, d_k\}$  to refer to a multicast flow containing  $k$  unicast flows with source,  $s$ , and data sinks  $d_1, d_2, \dots, d_k$ . The unicast flows are between  $s$  and each  $d_1, d_2, \dots, d_k$ . Each multicast flow,  $f = s, \{d_1, d_2, \dots, d_k\}$ , has  $k$  end-to-end per-packet delay requirements, one for each of  $f$ 's data sinks. Let  $F$  be the set of all multicast flows in  $G$ .

We define multicast flows inductively using  $T_i \in T$ . Starting at the source/root,  $s$ ,  $T_i$  has a multicast flow for each of  $s$ 's outgoing links  $(s, x) \in T_i$ . For link  $(s, x)$  between  $s$  and its one-hop neighbor  $x$ , the multicast flow contains all  $T_i$  unicast flows that traverse  $(s, x)$ . For example, the Figure 3.1(a) multicast tree has a single multicast flow  $(a, \{e, f, g\})$  at  $a$ . Only a single multicast flow is needed because  $a$  has only one outgoing link in its multicast tree.

At internal  $T_i$  nodes, additional multicast flows are instantiated when  $T_i$  branches. Internal node  $v \in T_i$ , instantiates a new multicast flow for each of  $v$ 's outgoing links (except for the link connecting  $v$  with its parent node in  $T_i$ ). For outgoing link  $(v, u) \in T_i$ ,  $v$ 's newly instantiated multicast flow represents  $T_i$ 's unicast flows that traverse  $(v, u)$ . In Figure 3.1(a), the  $a, \{e, f, g\}$  flow splits when the tree branches at  $b$  into multicast flows  $a, \{e, f\}$  and  $a, \{g\}$ . Likewise, multicast flow  $a, \{e, f\}$  splits into multicast flows  $a, \{e\}$  and  $a, \{f\}$  at  $c$ .

In keeping with its role as a general framework providing necessary services for programmable networks, OpenFlow does not explicitly provide an implementation for multicast and multicast flows. Instead, OpenFlow switches support a *group table* abstraction that is principally used to implement multicast [41]. Akin to flow table entries for unicast flows, group tables consist of group entries. Each group entry matches incoming packets based on a packet's group ID field – packets are expected to have a unique group ID value in its header – and when appropriate (i.e., when the multicast tree branches at the switch being considered) clones the packet to be sent

out along each of the switch’s outgoing links in the multicast tree.<sup>4</sup> This how the concept of “splitting” a flow (introduced in the previous paragraph) is implemented.

One way to implement multicast in OpenFlow is to leverage existing IP multicast protocols as detailed by Kotani et al. [33]. In this approach, the controller assigns a unique group ID to each multicast tree and creates a group table entry, that uses the group ID, at each switch along the multicast tree. Meanwhile, the sender and its first-hop switch use IGMP to set up and manage the controller-generated group IDs. Finally, the sender embeds the group ID in each multicast packet’s destination field, allowing for each switch in the multicast tree to identify and forward multicast packets appropriately.

We consider the case where multiple links fail over the lifetime of the network but assume that only a *single link fails at-a-time*. We call the current lossy or faulty link,  $\ell$ . When  $\ell$  fails, all sink nodes corresponding to any multicast flow that traverses  $\ell$  no longer receive packets from the source. As a result, the per-packet delay requirements of each these data sinks is not met. We refer to these data sinks, multicast flows, and the MT associated with each such flow as *directly affected*. In Figure 3.1,  $a, \{e, f\}$  is directly affected by  $(b, c)$  failing, along with data sinks  $e$  and  $f$ .

### 3.3.2 Overview of Our Recovery Solutions and Section Outline

We propose an algorithm, APPLESEED, that is run at the OpenFlow controller to make multicast trees robust to link failures by monitoring and detecting failed links, precomputing backup multicast trees, and installing backup multicast trees after a link failure.<sup>5</sup> As input, APPLESEED is given an undirected graph containing OpenFlow switches; the set of all multicast trees ( $T$ ); the set of all active multicast

---

<sup>4</sup>In addition to the group ID, a group entry can optionally match packets using patterns defined over other packet header fields (in the same way we saw with flow entries) such as the source address.

<sup>5</sup>The name APPLESEED is inspired by Johnny Appleseed, the famous American pioneer and conservationist known for planting apple nurseries and caring for its trees.

flows ( $F$ ); the length of each sampling window,  $w$ , used to monitor links and specified in units of time; and, for each multicast flow, a packet loss condition for each link the flow traverses. For now, we restrict packet loss conditions to be threshold-based that indicate the maximum number of packets that can be lost over  $w$  time units. The output of APPLESEED is a new set of precomputed backup multicast trees installed in the network and a set of uninstalled multicast trees. All  $T_i \in T$  that use the failed link are uninstalled and we call each such  $T_i$  a *failed multicast tree*.

We define a *backup multicast tree* for link  $\ell$  and  $T_i \in T$  as a multicast tree that has a path between the source,  $s \in T_i$ , and each data sink  $d \in T_i$  that: (a) connects  $s$  and  $d$  but does not traverse  $\ell$  and (b) satisfies  $d$ 's per-packet delay requirements. We refer to any multicast tree that satisfies these conditions for  $\ell$  a *backup multicast tree for  $\ell$*  or backup MT for short. In Figure 3.1(b), notice that the installed backup tree has paths  $a \rightarrow b \rightarrow d \rightarrow g \rightarrow h \rightarrow \{e, f\}$  connecting  $a$  with  $\{e, f, g\}$  after  $(b, c)$  fails.

APPLESEED divides into three parts:

1. Monitor to detect link failure (e.g.,  $(b, c)$  in Figure 3.1).
2. Uninstall all trees using the failed link (i.e., failed trees) and install a precomputed backup multicast tree for each uninstalled tree. For each data sink that was disconnected from the root because of the link failure, the backup tree should use a path that routes around the failed link. Note that the newly installed tree will likely require changes to several switches upstream from  $\ell$ , in addition to those at the upstream and downstream ends of link  $\ell$ . Recall in the Figure 3.1 example, data sinks  $\{e, f\}$  are reconnected with  $a$  in the installed backup tree.
3. Part (2) triggers the computation of a new backup tree for each (backup) tree installed in (2).

APPLESEED uses an OpenFlow-based subroutine (FAILED-LINK) for part (1) and is presented in Section 3.3.3. For part (2), we briefly describe APPLESEED’s steps to uninstall and install multicast trees in Section 3.3.4. In Section 3.3.5, we address part (3) by proposing a set of algorithms that compute backup multicast trees.

### 3.3.3 Link Failure Detection using OpenFlow

In this section, we propose a simple algorithm (FAILED-LINK), used by APPLESEED, that monitors links *inside* the network to detect any packet loss. To help explain FAILED-LINK, we use the example scenario from Section 3.3.1 and refer to a generic multicast tree with an upstream node,  $u$ , and downstream node,  $d$ .

FAILED-LINK is run at the OpenFlow controller and provides accurate packet loss measurements that are the basis for identifying lossy links. Informally, a lossy link is one that fails to meet the packet loss conditions specified by the controller. We refer to such a link as *failed*. Although APPLESEED is ultimately concerned with meeting the per-packet *delay* requirements of PMU applications, we use packet loss (as opposed to delay) as an indicator for a failed link because OpenFlow provides no native support for timers.

FAILED-LINK has the same input as APPLESEED, specified in Section 3.3.2. The output of FAILED-LINK is any link that has lost packets not meeting the packet loss condition of any multicast flow traversing the link. In the remainder of this document, we assume all flows are multicast and just use *flow* to refer to a multicast flow, unless otherwise specified.

Recall from Section 3.2.2 that each OpenFlow switch maintains a flow table, where each entry contains a match rule (i.e., an expression defined over the packet header fields used to match incoming packets) and action (e.g., “send packet out port 787”). For each packet that arrives at an OpenFlow switch, it is first matched to a flow entry,  $e$ , based on the packet’s header fields; then  $e$ ’s packet counter is incremented;

and, lastly,  $e$ 's action is executed on the packet.<sup>6</sup> Note that for our purposes all flow entries are for multicast flows. FAILED-LINK uses these packet counter values to compute per-flow packet loss between two switches over  $w$  time units.

FAILED-LINK uses the subroutine, PCOUNT, to measure the packet loss between an upstream node ( $u$ ) and downstream node ( $d$ ). PCOUNT does so at the per-flow granularity over a specified sampling window,  $w$ , where  $w$  is the length of time packets are counted at  $u$  and  $d$ . For each window of length  $w$ , PCOUNT computes packet loss for a flow  $f$ , that traverses  $u$  and  $d$ , using the following steps:

1. **At  $u$ , tags and counts all  $f$  packets.** We assume, before any changes are made,  $u$  uses flow entry  $e$  to match and forward  $f$  packets. PCOUNT creates a new flow entry,  $e'$ , that is an exact copy of  $e$ , except that  $e'$  embeds a version number (i.e., the tag) in the packet's VLAN field.<sup>7</sup>  $e'$  is installed with a higher priority than  $e$ . In OpenFlow, each flow entry has a corresponding priority specified upon its installation. Incoming packets are matched against flow entries in priority order, with the first matching entry being used. In this way, setting a higher priority for  $e'$  than  $e$ , ensures that  $u$  tags all  $f$  packets when  $e'$  is installed.
2. **Counts all tagged  $f$  packets received at  $d$ .** PCOUNT does so by installing a new flow entry at  $d$  that matches packets based on the VLAN tag applied at  $u$ .
3. **After  $w$  time units, turns tagging off at  $u$ .** To do so, PCOUNT simply switches the priority of  $e'$  and  $e$  at  $u$ .

---

<sup>6</sup>Not all switches necessarily use OpenFlow. In fact, we anticipate that in practice many switches will not support OpenFlow. For ease of presentation, this section assumes all switches are OpenFlow-enabled.

<sup>7</sup>Note that the VLAN id is one of many fields from packets that can be used to match against flow entries.

4. **Queries  $u$  and  $d$  for packet counts.** Specifically, the controller uses the OpenFlow protocol retrieve  $u$  and  $d$ 's packet count values for packets tagged by  $e'$ . To ensure that all in-transit packets are considered, PCOUNT waits “long enough” (e.g., time proportional to the average per-packet delay between  $u$  and  $d$ ) for in-transit packets to reach  $d$ , before reading  $d$ 's packet counter.
5. **Computes packet loss.** The controller computes packet loss by simply subtracting  $d$ 's packet count from  $u$ 's.

In practice, PCOUNT executes step (2) before step (1) to ensure that  $u$  and  $d$  consider the same set of packets.

In the Figure 3.1 example, the controller uses FAILED-LINK to measure the packet loss for the  $a, \{e, f\}$  flow. We assume for link  $(b, c)$  and the  $a, \{e, f\}$  flow, FAILED-LINK is given a maximum packet loss threshold of 10 packets over  $w$  time units. For each sampling window of  $w$  time units, PCOUNT instructs  $b$  to tag and count all packets corresponding to  $a, \{e, f\}$ . At the same time,  $c$  is instructed by PCOUNT to count the  $a, \{e, f\}$  packets tagged by  $b$ . Then, the controller uses the OpenFlow protocol to query the packet counter values for  $a, \{e, f\}$  at  $b$  and  $c$ . When  $(b, c)$  fails, the packet counter at  $c$  for  $a, \{e, f\}$  no longer increments, causing a violation of  $a, \{e, f\}$ 's packet loss threshold for  $(b, c)$ .

As specified, FAILED-LINK measures packet loss for each *multicast flow* at each link. These flow-level measurements may obfuscate aggregate link-level packet loss. For this reason, we plan to extend FAILED-LINK to group flows together to enable *aggregate* packet loss measurements. Because OpenFlow provides native support for grouping flows and maintains packet counters for each group, FAILED-LINK can be easily extended to group and count packets for any subset of multicast flows traversing the same switch.

PCOUNT's approach for ensuring consistent reads of packet counters bears strong resemblance to the idea of *per-packet consistency* introduced by Reitblatt et al. [43].



Per-packet consistency ensures that when a network of switches change from an old policy to a new one, that each packet is guaranteed to be handled exclusively by one policy, rather than some combination of the two policies. In our case, we use per-packet consistency to ensure that when PCOUNT reads  $u$  and  $d$ 's packet counters, exactly the same set of packets are considered, excluding, of course, packets that are dropped at  $u$  or dropped along the path from  $u$  to  $d$ .

### 3.3.4 Uninstalling Failed Trees and Installing Backup Trees

After FAILED-LINK detects  $\ell$ 's failure, APPLESEED uninstalls all MTs that contain  $\ell$  (i.e., failed trees) and installs a precomputed backup multicast tree for each of these uninstalled tree. Installing backup trees for  $\ell$ , denoted  $T_\ell$ , triggers the computation of new backup trees. A backup MT is needed for each  $T_j \in T_\ell$  and for each of  $T_j$ 's links. Here we only explain how MTs are uninstalled and installed and describe some of side effects of doing so. We postpone explaining how backup trees are computed until Section 3.3.5.

Uninstalling or installing a multicast tree,  $T_i$ , is simple with OpenFlow. The controller sends an instruction to each switch in  $T_i$  to remove (add) the flow entry corresponding to  $T_i$ . Starting at the root and ending at the leaf nodes, flow entries are removed top-down to prevent  $T_i$  traffic from being sent while  $T_i$  is being uninstalled. In contrast, flow entries are installed bottom-up, starting at the leaf nodes and finishing at the root. This ensures that when the root node begins to disseminate data using  $T_i$  that all downstream  $T_i$  nodes are equipped with the necessary flow entries to correctly forward  $T_i$  traffic.

Increased traffic caused by newly installed backup trees may introduce packet loss to multicast flows that do not traverse  $\ell$  but do use a path shared by at least one switch in a backup MT. We refer to these flows as *indirectly affected*. Additionally, we refer to any packet or data sink corresponding to an indirectly affected flow as indirectly

affected. In our Figure 3.1 example,  $a, \{g\}$  is indirectly affected when the backup MT is installed because the backup MT uses paths  $a \rightarrow b \rightarrow d \rightarrow g \rightarrow h \rightarrow \{e, f\}$ .

### 3.3.5 Computing Backup Multicast Trees

Here we present a set of algorithms that compute backup MTs. APPLESEED uses these algorithms in two scenarios. First, as a part of system initialization where a set of backup MTs are computed for each network link,  $l$ ; APPLESEED computes a single backup MT for each MT that would be directly affected by  $l$ 's failure.

Second, APPLESEED triggers the execution of backup tree computations after backup trees,  $T_\ell$ , are installed in response to the most recent link failure,  $\ell$ . APPLESEED reruns the entire computation (as opposed to only computing backup MTs for the newly installed  $T_\ell$  trees): for each network link,  $l$ , APPLESEED computes a backup MT for each would-be directly affected MT if  $l$  failed. APPLESEED recomputes *all* backup MTs because installing  $T_\ell$  likely changes the network state in terms of the link- or node-disjointedness (or lack thereof) across all system MTs. Therefore, “currently” precomputed backup MTs risk becoming stale since the algorithms used to compute them considered an “old” network state in their optimization. *We hypothesize that recomputing all backup MTs each time a single link fails yields a more survivable data dissemination network than only recomputing backup MTs for newly installed backup MTs installed in response to the most recent link failure.*

APPLESEED uses one of the following backup tree computation algorithms: MIN-FLOWS, MIN-SINKS, or MIN-CONTROL. Next, we present initial sketches of each of these algorithms.

#### 3.3.5.1 Min-Flows Algorithm

Before outlining MIN-FLOWS, we provide a brief refresher on multicast flows, as defined in Section 3.3.1.2. There we stated that a multicast flow contains multiple unicast flows and only sends a single packet across a link. We used  $s, \{d_1, d_2, \dots, d_k\}$

to refer to a multicast flow containing  $k$  unicast flows with source,  $s$ , and data sinks  $d_1, d_2, \dots, d_k$ , such that the unicast flows are between  $s$  and each  $d_1, d_2, \dots, d_k$ . Finally, we specified that each multicast flow,  $f = s, \{d_1, d_2, \dots, d_k\}$ , has  $k$  end-to-end per-packet delay requirements, one for each of  $f$ 's data sinks.

#### MIN-FLOWS ALGORITHM

- Input:  $(G, T, F, l)$ , such that  $l$  is a link in  $G$  and each  $f \in F$  specifies the maximum per-packet delay it can tolerate.
- Output: A backup multicast tree for each MT using  $l$ . This set of backup MTs,  $T_l$ , are computed such that across *all network links*, the same number of flows traverse each link, under the condition that all multicast flows handled by each MT in  $T_l$  satisfy their end-to-end per-packet delay requirement.

The motivation for computing backup MTs in this manner is to reduce the impact (i.e., number of directly affected flows) of link failures that occur after  $l$  fails.

**Min-Flows Example.** To provide intuition for MIN-FLOWS, consider an augmented version of the example from Figure 3.1, in which the Figure 3.1 graph is a subgraph of a larger graph,  $G_1 = (V_1, E_1)$ . We assume the following initial system state: no  $E_1$  links have failed; 10 multicast flows traverse each  $E_1$  link; 9 MTs, in addition to the MT rooted at  $a$ , use link  $(b, c)$ ; and all end-to-end delay requirements are met. We assume that  $(b, c)$  is the the first link to fail and that  $(b, d)$  fails next, but only after the precomputed backup MTs for  $(b, c)$  have been installed. Let the goal of MIN-FLOWS in computing backup MTs for  $(b, c)$  be for all links to handle 11 multicast flows.

We compare the backup MTs MIN-FLOWS computes for link  $(b, c)$  with those computed by a simple Steiner-tree-based approach, STRAW-MAN-1:

- MIN-FLOWS: Let MIN-FLOWS compute backup MTs for  $(b, c)$  such that one of the 10 MTs uses  $(b, d)$ , while the other 9 backup MTs do not use  $(b, d)$ .

- STRAW-MAN-1: STRAW-MAN-1 computes backup MTs such that each MT is a Steiner tree approximation over  $G'_1 = (V_1, (E_1 \setminus \{(b, c)\}))$  with same root node and leaf nodes as the original MT. In this example, we assume that all of STRAW-MAN-1's backup MTs for  $(b, c)$  use  $(b, d)$ .

Now, consider the following sequence of events: first link  $(b, c)$  fails, then the backup MTs for  $(b, c)$  are installed, and, lastly, link  $(b, d)$  fails. Using MIN-FLOWS's backup MTs for  $(b, c)$ , only 11 flows are affected when  $(b, d)$  fails. However, 20 flows are directly impacted using STRAW-MAN-1's backup MTs for  $(b, c)$  because all 10 of these MTs use  $(b, d)$ , making 20 total MTs (and flows) that use  $(b, d)$  (recall that we assumed the initial state of the system was such that 10 multicast flows traverse each link in  $G_1$ ).

### 3.3.5.2 Min-Sinks Algorithm

Next, we present the MIN-SINKS algorithm. MIN-SINKS is closely related to but different from MIN-FLOWS. Both algorithms seek to minimize the disruption of future link failures but optimize different criteria towards achieving this goal.

Before specifying the input and output of MIN-SINKS, we remind the reader of previously specified notation:  $F$  is the set of all network flows and  $f = s, \{d_1, d_2, \dots, d_k\}$  denotes a multicast flow with  $k$  data sinks,  $d_1, d_2, \dots, d_k$ . For each link,  $l$ , we define  $s_l$ :

$$s_l = \sum_{\forall f \in F: f \text{ traverses } l} |k| \quad (3.1)$$

#### MIN-SINKS ALGORITHM

- Input:  $(G, T, F, l)$ , such that  $l$  is a link in  $G$  and each  $f \in F$  specifies the maximum per-packet delay it can tolerate.
- Output: A backup multicast tree for each MT using  $l$ . This set of backup MTs,  $T_l$ , are computed such that  $s_l$  is the same across all network links.

When link  $l$  fails, MIN-SINKS ensures that the same number of downstream data sinks are affected for the next link failure (independent of which link fails).

**Min-Sinks Example.** Consider again the MIN-FLOWS example scenario (Section 3.3.5.1), where we assumed that 10 multicast flows traverse each link in  $G_1$  before any link fails. Now we also assume the initial state of the system is such that the installed MTs ensure that for each link,  $l$ , multicast flows traverse  $l$  so that there are 20 downstream sink nodes from  $l$  (i.e.,  $s_l = 20$ ).

When  $(b, c)$  fails, MIN-SINKS's backup MTs ensure that each link has 22 downstream sink nodes. An alternative approach to MIN-SINKS, STRAW-MAN-2, computes backup MTs for  $(b, c)$  such that  $(b, d)$  handles multicast flows leading to 40 downstream sink nodes for  $(b, d)$ . If  $(b, d)$  fails after the backup MTs for  $(b, c)$  are installed, only 22 sink nodes are directly impacted using MIN-SINKS, while 40 data sinks are impacted with STRAW-MAN-2's backup MTs installed.

### 3.3.5.3 Min-Control Algorithm

Lastly, we outline the MIN-CONTROL algorithm. In effort to provide fast recovery, MIN-CONTROL minimizes the control overhead required to install backup MTs. We assume the control overhead is a function of the number of switches that need to change state (i.e., modify flow tables to uninstall failed MTs or install a backup MT) because the controller must send control signals to each of these switches.

#### MIN-CONTROL ALGORITHM

- Input:  $(G, T, F, l)$ , such that  $l$  is a link in  $G$  and each  $f \in F$  specifies the maximum per-packet delay it can tolerate.

- Output: A backup multicast tree for each MT using  $l$ . This set of backup MTs,  $T_l$ , are computed such that they minimize the *total* control overhead required by their installation.<sup>8</sup>

This is equivalent to minimizing the number of routers whose new configuration needs to be signaled. Intuitively, this ensures that backup trees are quickly installed, leading to a fast recovery (and ultimately reduces packet loss for all directly affected flows).

### 3.4 Chapter Conclusion and Future Work

In this final technical chapter, we considered the problem of recovery from link failures in a smart grid communication network. We presented the outline for an algorithm that uses OpenFlow to detect packet loss inside the network of switches and a set of algorithms to precompute backup multicast trees to be installed after a link fails. Our algorithms for computing backup multicast trees differ from those in the literature because each algorithm optimizes for the long-term survivability of the communication network.

For each algorithm proposed in the chapter (APPLESEED, FAILED-LINK, PCOUNT, MIN-FLOWS, MIN-SINKS, MIN-CONTROL), we plan to supplement our basic algorithm description with a detailed specification of the algorithm steps, implement the algorithm in OpenFlow, characterize its complexity, and evaluate its implementation through simulations.

Time permitting, we plan to propose algorithms for computing backup multicast trees that consider indirectly affected flows. Recall from Section 3.3.4 that indirectly affected flows are ones using a path that shares at least one link contained in a backup tree. As a result, indirectly affected flows may experience packet loss due to increased traffic from redirected flows. We conjecture that an algorithm that

---

<sup>8</sup>Note that MIN-CONTROL does not explicitly consider the control overhead of uninstalling failed MTs because this cost is bounded by the number of failed MTs, which is fixed for each link failure.

minimizes the number of indirectly affected flows reduces the system-wide affects (spatially) of installing backup multicast trees. A similar algorithm is possible that minimizes the number of indirectly affected data sinks.

## CHAPTER 4

### THESIS TIMELINE AND FUTURE WORK

In this chapter we provide a timeline of planned future work (Section 4.1) and briefly comment on additional topics for research that fall outside the scope of this thesis (Section 4.2).

#### 4.1 Planned Future Work and Timeline

Because the work described in Chapters 1 and 2 is complete, all planned future work is focused on completing the research proposed in Chapter 3. For each algorithm described in Chapter 3 – APPLESEED, FAILED-LINK, PCOUNT, MIN-FLOWS, MIN-SINKS, and MIN-CONTROL – we plan to supplement its basic description with a detailed specification of its algorithm steps, implement the algorithm in OpenFlow, and evaluate its implementation. We estimate this requires six months of steady work to complete.

We now provide a more detailed specification of thesis milestones and anticipated dates of completion:

1. Extend my unicast flow-based specification of FAILED-LINK to work for multi-cast flows. *(Feb.)*
2. Complete OpenFlow-based implementation for FAILED-LINK using the POX controller <sup>1</sup>. *(Feb.)*

---

<sup>1</sup><https://openflow.stanford.edu/display/ONL/POX+Wiki>



3. Use OpenFlow emulator, Mininet <sup>2</sup>, to test and profile FAILED-LINK. (*March*)
4. Provide detailed design and specification of MIN-FLOWS, MIN-SINKS, and MIN-CONTROL. (*March*)
5. Complete OpenFlow-based implementation for MIN-FLOWS, MIN-SINKS, and MIN-CONTROL using POX controller. (*April*)
6. Complexity analysis of MIN-FLOWS, MIN-SINKS, and MIN-CONTROL. (*April*)
7. Run simulations to evaluate MIN-FLOWS, MIN-SINKS, and MIN-CONTROL using Mininet. (*May*)
8. Write conference paper based on Chapter 3 research. (*June*)

Throughout this process, I plan to write the remaining sections of the last technical thesis chapter as dictated by the results derived from each step specified above.

## 4.2 Future Work Outside the Scope of this Thesis

In this section, we comment on topics for future work that will not be considered as a part of this thesis.

- **Chapter 1.** One challenging problem is to find the worst possible false state a compromised node can inject. Some options include the minimum distance to all nodes (e.g., our choice for false state used in Chapter 1), state that maximizes the effect of the count-to-infinity problem, and false state that contaminates a bottleneck link.
- **Chapter 2.** The success of the greedy algorithms suggests that the IEEE bus systems have special topological characteristics. Finding and investigating

---

<sup>2</sup><http://yuba.stanford.edu/foswiki/bin/view/OpenFlow/Mininet>

these properties could be a fruitful exercise that might provide more insight into why **greedy** and **xvgreedy** yield such encouraging results. Additionally, a valuable contribution would be to implement the integer programming approach proposed by Xu and Abur [48] to solve FULLOBSERVE, as this would provide valuable data points to measure the relative performance of **greedy**.

- **Chapter 3.** Because our algorithms for backup multicast tree computation are not fully specified, implemented, nor evaluated, we are unable to comment on any future work related to this chapter.

## BIBLIOGRAPHY

- [1] GT-ITM. <http://www.cc.gatech.edu/projects/gtitm/>.
- [2] Northeast blackout of 2003. [http://en.wikipedia.org/wiki/Northeast\\_blackout\\_of\\_2003](http://en.wikipedia.org/wiki/Northeast_blackout_of_2003).
- [3] Rocketfuel. <http://www.cs.washington.edu/research/networking/rocketfuel/maps/weights/weights-dist.tar.gz>.
- [4] Aazami, A., and Stilp, M.D. Approximation Algorithms and Hardness for Domination with Propagation. *CoRR abs/0710.2139* (2007).
- [5] Almes, G., Kalidindi, S., and Zekauskas, M. A one-way packet loss metric for ippm. Tech. rep., RFC 2680, September, 1999.
- [6] Ammann, P., Jajodia, S., and Liu, Peng. Recovery from Malicious Transactions. *IEEE Trans. on Knowl. and Data Eng.* 14, 5 (2002), 1167–1185.
- [7] Bakken, D.E., Bose, A., Hauser, C.H., Whitehead, D.E., and Zweigle, G.C. Smart generation and transmission with coherent, real-time data. *Proceedings of the IEEE* 99, 6 (2011), 928–951.
- [8] Baldwin, T.L., Mili, L., Boisen, M.B., Jr., and Adapa, R. Power System Observability with Minimal Phasor Measurement Placement. *Power Systems, IEEE Transactions on* 8, 2 (May 1993), 707–715.
- [9] Barford, P., and Sommers, J. Comparing probe-and router-based packet-loss measurement. *Internet Computing, IEEE* 8, 5 (2004), 50–56.
- [10] Bertsekas, D., and Gallager, R. *Data Networks*. Prentice-Hall, Inc., Upper Saddle River, NJ, USA, 1987.
- [11] Birman, K.P., Chen, J., Hopkinson, E.M., Thomas, R.J., Thorp, J.S., Van Renesse, R., and Vogels, W. Overcoming communications challenges in software for monitoring and controlling power systems. *Proceedings of the IEEE* 93, 5 (2005), 1028–1041.
- [12] Bobba, R., Heine, E., Khurana, H., and Yardley, T. Exploring a tiered architecture for NASPInet. In *Innovative Smart Grid Technologies (ISGT), 2010* (2010), IEEE, pp. 1–8.

- [13] Brueni, D. J., and Heath, L. S. The PMU Placement Problem. *SIAM Journal on Discrete Mathematics* 19, 3 (2005), 744–761.
- [14] Cáceres, R., Duffield, N.G., Horowitz, J., and Towsley, D.F. Multicast-based inference of network-internal loss characteristics. *Information Theory, IEEE Transactions on* 45, 7 (1999), 2462–2480.
- [15] Casado, M., Freedman, M.J., Pettit, J., Luo, J., McKeown, N., and Shenker, S. Ethane: Taking control of the enterprise. In *ACM SIGCOMM Computer Communication Review* (2007), vol. 37, ACM, pp. 1–12.
- [16] Chen, J., and Abur, A. Placement of PMUs to Enable Bad Data Detection in State Estimation. *Power Systems, IEEE Transactions on* 21, 4 (2006), 1608–1615.
- [17] Chenine, M., Zhu, K., and Nordstrom, L. Survey on priorities and communication requirements for pmu-based applications in the nordic region. In *PowerTech, 2009 IEEE Bucharest* (2009), IEEE, pp. 1–8.
- [18] Cui, J.H., Faloutsos, M., and Gerla, M. An architecture for scalable, efficient, and fast fault-tolerant multicast provisioning. *Network, IEEE* 18, 2 (2004), 26–34.
- [19] De La Ree, J., Centeno, V., Thorp, J.S., and Phadke, A.G. Synchronized Phasor Measurement Applications in Power Systems. *Smart Grid, IEEE Transactions on* 1, 1 (2010), 20–27.
- [20] Dijkstra, E., and Scholten, C. Termination Detection for Diffusing Computations. *Information Processing Letters*, 11 (1980).
- [21] El-Arini, K., and Killourhy, K. Bayesian Detection of Router Configuration Anomalies. In *MineNet '05: Proceedings of the 2005 ACM SIGCOMM workshop on Mining network data* (New York, NY, USA, 2005), ACM, pp. 221–222.
- [22] Feamster, N., and Balakrishnan, H. Detecting BGP Configuration Faults with Static Analysis. In *2nd Symp. on Networked Systems Design and Implementation (NSDI)* (Boston, MA, May 2005).
- [23] Fei, A., Cui, J., Gerla, M., and Cavendish, D. A “dual-tree” scheme for fault-tolerant multicast. In *Communications, 2001. ICC 2001. IEEE International Conference on* (2001), vol. 3, IEEE, pp. 690–694.
- [24] Feldmann, A., and Rexford, J. IP Network Configuration for Intradomain Traffic Engineering. *IEEE Network Magazine* 15 (2001), 46–57.
- [25] Friedl, A., Ubik, S., Kapravelos, A., Polychronakis, M., and Markatos, E. Realistic passive packet loss measurement for high-speed networks. *Traffic Monitoring and Analysis* (2009), 1–7.

- [26] Garcia-Lunes-Aceves, J. J. Loop-free Routing using Diffusing Computations. *IEEE/ACM Trans. Netw.* 1, 1 (1993), 130–141.
- [27] Gyllstrom, D., Rosensweig, E., and Kurose, J. On the impact of pmu placement on observability and cross-validation. In *Proceedings of the 3rd International Conference on Future Energy Systems: Where Energy, Computing and Communication Meet* (2012), ACM, p. 20.
- [28] Gyllstrom, D., Vasudevan, S., Kurose, J., and Miklau, G. Efficient recovery from false state in distributed routing algorithms. In *Networking* (2010), pp. 198–212.
- [29] Gyllstrom, D., Vasudevan, S., Kurose, J., and Miklau, G. Recovery from False State in Distributed Routing Algorithms. Tech. Rep. UM-CS-2010-017, University of Massachusetts Amherst, 2010.
- [30] Haynes, T. W., Hedetniemi, S. M., Hedetniemi, S. T., and Henning, M. A. Domination in Graphs Applied to Electric Power Networks. *SIAM J. Discret. Math.* 15 (April 2002), 519–529.
- [31] Hopkinson, K., Roberts, G., Wang, X., and Thorp, J. Quality-of-service considerations in utility communication networks. *Power Delivery, IEEE Transactions on* 24, 3 (2009), 1465–1474.
- [32] Jefferson, D. Virtual Time. *ACM Trans. Program. Lang. Syst.* 7, 3 (1985), 404–425.
- [33] Kotani, D., Suzuki, K., and Shimonishi, H. A design and implementation of openflow controller handling ip multicast with fast tree switching. In *Applications and the Internet (SAINT), 2012 IEEE/IPSJ 12th International Symposium on* (2012), IEEE, pp. 60–67.
- [34] Lichtenstein, D. Planar Formulae and Their Uses. *SIAM J. Comput.* 11, 2 (1982), 329–343.
- [35] Liu, P., Ammann, P., and Jajodia, S. Rewriting Histories: Recovering from Malicious Transactions. *Distributed and Parallel Databases* 8, 1 (2000), 7–40.
- [36] McKeown, Nick, Anderson, Tom, Balakrishnan, Hari, Parulkar, Guru M., Peterson, Larry L., Rexford, Jennifer, Shenker, Scott, and Turner, Jonathan S. Openflow: enabling innovation in campus networks. *Computer Communication Review* 38, 2 (2008), 69–74.
- [37] Médard, M., Finn, S.G., Barry, R.A., and Gallager, R.G. Redundant trees for preplanned recovery in arbitrary vertex-redundant or edge-redundant graphs. *IEEE/ACM Transactions on Networking (TON)* 7, 5 (1999), 641–652.
- [38] Mili, L., Baldwin, T., and Adapa, R. Phasor Measurement Placement for Voltage Stability Analysis of Power Systems. In *Decision and Control, 1990., Proceedings of the 29th IEEE Conference on* (Dec. 1990), pp. 3033–3038 vol.6.

- [39] Mohan, C., Haderle, D., Lindsay, B., Pirahesh, H., and Schwarz, P. ARIES: A Transaction Recovery Method Supporting Fine-Granularity Locking and Partial Rollbacks Using Write-Ahead Logging. *ACM Trans. Database Syst.* 17, 1 (1992), 94–162.
- [40] Neumann, R. Internet routing black hole. *The Risks Digest: Forum on Risks to the Public in Computers and Related Systems* 19, 12 (May 1997).
- [41] Pfaff, B., et al. Openflow switch specification version 1.1.0 implemented (wire protocol 0x02), 2011.
- [42] Pointurier, Y. Link failure recovery for mpls networks with multicasting. Master’s thesis, University of Virginia, 2002.
- [43] Reitblatt, M., Foster, N., Rexford, J., and Walker, D. Consistent updates for software-defined networks: Change you can believe in! In *Proceedings of the 10th ACM Workshop on Hot Topics in Networks* (2011), ACM, p. 7.
- [44] School, K., and Westhoff, D. Context Aware Detection of Selfish Nodes in DSR based Ad-hoc Networks. In *Proc. of IEEE GLOBECOM* (2002), pp. 178–182.
- [45] Vanfretti, L. *Phasor Measurement-Based State-Estimation of Electrical Power Systems and Linearized Analysis of Power System Network Oscillations*. PhD thesis, Rensselaer Polytechnic Institute, December 2009.
- [46] Vanfretti, L., Chow, J. H., Sarawgi, S., and Fardanesh, B. (B.). A Phasor-Data-Based State Estimator Incorporating Phase Bias Correction. *Power Systems, IEEE Transactions on* 26, 1 (Feb 2011), 111–119.
- [47] Wu, C.S., Lee, S.W., and Hou, Y.T. Backup vp preplanning strategies for survivable multicast atm networks. In *Communications, 1997. ICC 97 Montreal, 'Towards the Knowledge Millennium'. 1997 IEEE International Conference on* (1997), vol. 1, IEEE, pp. 267–271.
- [48] Xu, B., and Abur, A. Observability Analysis and Measurement Placement for Systems with PMUs. In *Proceedings of 2004 IEEE PES Conference and Exposition, vol.2* (2004), pp. 943–946.
- [49] Xu, B., and Abur, A. Optimal Placement of Phasor Measurement Units for State Estimation. Tech. Rep. PSERC Publication 05-58, October 2005.
- [50] Yardley, J., and Harris, G. 2nd day of power failures cripples wide swath of india, July 31, 2012. [http://www.nytimes.com/2012/08/01/world/asia/power-outages-hit-600-million-in-india.html?pagewanted=all&\\_r=1&](http://www.nytimes.com/2012/08/01/world/asia/power-outages-hit-600-million-in-india.html?pagewanted=all&_r=1&).
- [51] Zhang, J., Welch, G., and Bishop, G. Observability and Estimation Uncertainty Analysis for PMU Placement Alternatives. In *North American Power Symposium (NAPS), 2010* (2010), pp. 1–8.